Dicalcium ferrite: a chemical heat pump in integrated carbon capture and chemical looping combustion for the steel industry

Made Santihayu Sukma[1], Yaoyao Zheng[1,2], Stuart Ashley Scott[1]**

[1]Department of Engineering, University of Cambridge, Trumpington Street, Cambridge, CB2 1PZ, United Kingdom

[2]Faculty of Engineering, University of Nottingham, Triump Road, Nottingham, NG8 1BB, United Kingdom

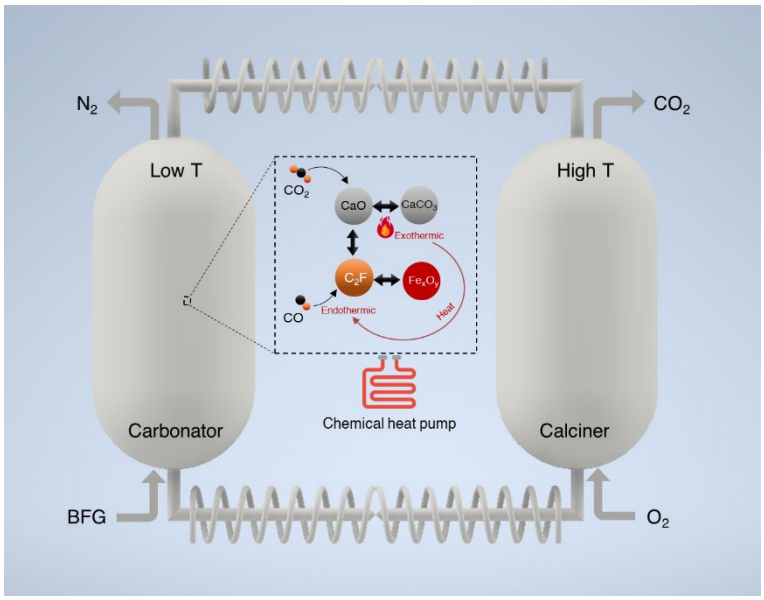
*Email: sas37@cam.ac.uk; Phone: (+44) 1223 3 32645

Key words: blast furnace gas, steel industry, chemical heat pump, carbon capture, chemical looping

Abstract

An integrated calcium and chemical looping combustion using dicalcium ferrite ($Ca_2Fe_2O_5$, C_2F), a mixed phase from iron and calcium oxides, is proposed here to remove carbon ($CO + CO_2$) contained in the blast furnace gas from the steel industry. C_2F is particularly attractive in chemical looping hydrogen production due to its lower P_{O_2}, therefore C_2F can split steam into H_2. Here, the low P_{O_2} property allows C_2F to have endothermic combustions in CO and H_2 combustion (Stage 1 in the carbonator). The heat of combustion is chemically stored as reduced-carbonated C_2F to be utilised for sorbent regeneration (Stage 2 in the calciner), essentially pumping the heat from the carbonator to the calciner. Combustion that occurred at

P_{CO}/P_{CO_2} of the typical BFG in which the C_2F should have not been able to combust CO, suggesting an enhanced combustion phenomenon. Experiments demonstrated in a fluidised bed and a thermogravimetric analyser led to indications that rather than following reaction pathways in an order of (i) C_2F is reduced into CaO and metallic Fe and (ii) the CaO is absorbed CO_2 in Stage 1, C_2F might directly form Fe + $CaCO_3$ under a mixture of CO and CO_2, allowing the C_2F to react with BFG. Reincorporation of the reduced-carbonated oxides into C_2F drives lower decarbonation temperatures compared to CaO alone, suggesting a promising route to improve energy efficiency in capturing carbon in the hard-to-decarbonise steel industry.



Graphical abstract

1. Introduction

An integrated blast furnace and basic oxygen furnace process (BF-BOF) is the most common steel manufacturing process, i.e., ~75% of the total global steel was produced via this route [1]. It relies heavily on coal both as the energy supplier as well as feedstock to reduce iron ore; thus, it is carbon intensive [2,3]. In fact, the steel industry is the largest industrial coal consumer [4]. Shifting the fuel to a greener option such as hydrogen (via direct reduction of

iron, DRI) is feasible, but is a longer-term solution as it requires renewable and abundant sources of H_2. Capturing carbon from the steel industry is the most promising medium-term pathway since the facilities can be retrofitted to the existing system.

The current BF-BOF process comprises three stages, i.e., coke production, iron making in the blast furnace, and steel production in the converter. Each generates a different gaseous effluent, i.e., coke gas, blast furnace gas (BFG), and converter gas (BOF), respectively. BFG is the most problematic since it contains most of the carbon (i.e., 60 – 80%) from the BF-BOF process [5]. Whilst fuels remain in the BFG, i.e., CO (19 – 27%) and H_2 (1 – 8%), these are contaminated with N_2 (44 – 58%) and CO_2 (16 – 26%) [1,2,5,6]. Carbon capture using amines or oxyfuel combustion alone is not sufficient. A simultaneous process where CO is combusted to CO_2 and subsequently CO_2 is captured is needed.

High-temperature looping processes for carbon capture, such as calcium looping [7,8] and chemical looping combustion [9–11], have a much lower energy penalty than first-generation carbon capture techniques, mainly owing to being able to integrate the heat they reject into a power cycle. Ca-looping uses CaO rather than an amine to remove CO_2, and is constrained by the chemical equilibrium of

$$\mathrm{CaO_{(s)} + CO_{2(g)} \rightleftharpoons CaCO_{3(s)}} \qquad \Delta H^{\circ}_{873K} = -171.3\ \mathrm{kJ/mol} \qquad \textbf{(R-1)}.$$

Though other high-temperature materials have been considered, CaO is the most widely studied high-temperature sorbent [12]. It is relatively cheap and abundant, and many have argued that natural limestone can be utilised [13–15]. Though sorbents usually deactivate over cycles, this can be overcome by using supported materials [16,17], or by integrating the use of the sorbent with cement [18] or iron production [19]. The equilibrium of **R-1** imposes limits on both the calcination and carbonation stages. To achieve a pure CO_2 stream at atmospheric pressure, the temperature has to be ~900 °C to achieve an equilibrium P_{CO_2} of 1 bar [20]. The carbonation

must run at a lower temperature (at a total pressure of 1 bar) as the outlet is constrained by the P_{CO_2} for **R-1**, which is, for example, 0.004 bar [8] or 0.0032 bar [20] at 600 °C. The fact that the calciner must run hotter than the carbonator means that extra fuel must be supplied to the hotter calciner, along with pure oxygen. All this heat is then recovered from the temperature calciner and sent to a power cycle [21]. It is therefore not possible to run autothermally without, for example, using a pressure swing system [22].

Metal oxide looping (often known as chemical looping combustion) is a different kind of high-temperature cycle that uses a metal oxide to provide oxygen and hence is a form of oxygen combustion. Chemical looping combustion allows air to be used as the oxidant and avoids the need for an air separation unit, again lowering the energy penalty [23]. Various materials have been suggested as oxygen looping materials, often oxides of transition metals, e.g., Fe, Ni, Mn, Cu, often with a support material, to overcome difficulties with cyclic stability. Some favour natural ores [24–28] as these are cheap and abundant. Iron and copper also have the advantage of being environmentally benign.

With high-temperature processes, it is possible to combine metal oxide looping and CaO sorption, thus allowing the BFG to be both combusted and the carbon captured. **Fig. 1** shows an adapted calcium looping process using materials which can both capture CO_2 and also combust carbon-containing fuels. As with Ca-looping, it consists of two stages, (i) reductive-carbonation at a lower temperature in the carbonator and (ii) oxidative-calcination at a higher temperature in the calciner. Any process which uses carbonation of CaO will require additional heat input into the calciner to reverse the reaction. In a traditional looping Ca-lopping process, this means adding supplemental fuel and oxy-firing. Here, the energy contained in the BFG (*ca.* ~80 kJ/mol-BFG) is roughly sufficient to allow an autothermal process (if all carbon, including CO, is captured as CO_2 and calcium looping alone is utilised). This proposed system

requires a material or combination of materials which facilitate CO_2 capture (calcium looping) and oxygen transfer (metal oxide looping).

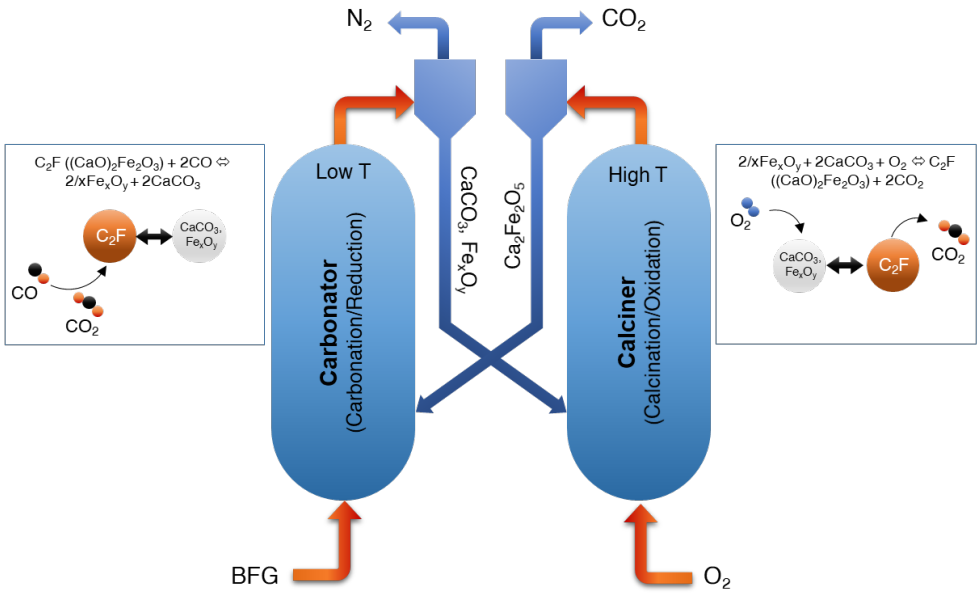


Figure 1 Schematic diagram of the integrated CaL-CLC.

A similar approach, integrated calcium and chemical looping combustion (CaL-CLC) has been proposed for carbon capture applications [29–32]. CaO acts as the sorbent, whilst the metal oxide, typically CuO, provides the oxygen to combust the supplementary fuel. The use of pure oxygen is avoided by the chemical looping, which regenerates the metallic copper back to CuO using air. Three reactors are needed, carbonation, calcination, and oxidation. Various configurations are possible, and heat from reducing the metal oxide in the calciner can be used to drive the calcination. In this case, oxides which reduce exothermically, like copper oxide, are ideal. However, in the scheme shown in **Fig. 1**, oxygen-looping materials like copper oxide would not be able to fully utilise the heat of CO/H_2 combustion to drive the calcination. Around half of the heat from combusting the fuels would be extracted in the carbonator since CuO reacts exothermically with CO or H_2 ($\Delta H^0 = -133$ and -100 kJ/mol-fuel at 650 °C, respectively) [33].

An alternative approach would be to use an oxygen carrier which combusts the fuels (CO/H_2) endothermically in the carbonator. This not only allows the full heat of combustion of the fuels to be released in the calciner, but can also absorb some heat released from the carbonation for use in the calciner. In subsequent calcination, this heat is transferred via exothermic oxidation of the reduced oxides. The oxygen-looping material essentially acts as a chemical heat pump transferring heat from the colder carbonator to the warmer calciner. In this work, an oxygen carrier which performs the endothermic reduction in CO or H_2 is investigated. The heat of reaction with CO or H_2 is linked to the thermodynamic properties of an oxygen carrier (denoted here as 'MeO'), and, in particular, the enthalpy of lattice oxygen release in

$$MeO_{(s)} \leftrightharpoons Me_{(s)} + \frac{1}{2}O_{2\,(g)} \qquad \textbf{(R-2)}$$

R-2 determines the oxygen partial pressure at the equilibrium of

$$0.5 \ln P_{O_2} = -\frac{\Delta H_{O_2}}{RT} + \frac{\Delta S_{O_2}}{R} \qquad \textbf{(Eq. 1)}$$

where P_{O_2}, ΔH_{O_2} and ΔS_{O_2} are the equilibrium oxygen partial pressure, standard enthalpy, and entropy of **R-2**. The heat of reaction, ΔH_{R-3} for the combustion of CO, or H_2, by a metal oxide in

$$MeO_{(s)} + CO[\text{or } H_2]_{(g)} \leftrightharpoons Me_{(s)} + CO_2\ [\text{or } H_2O]_{(g)} \qquad \textbf{(R-3)}$$

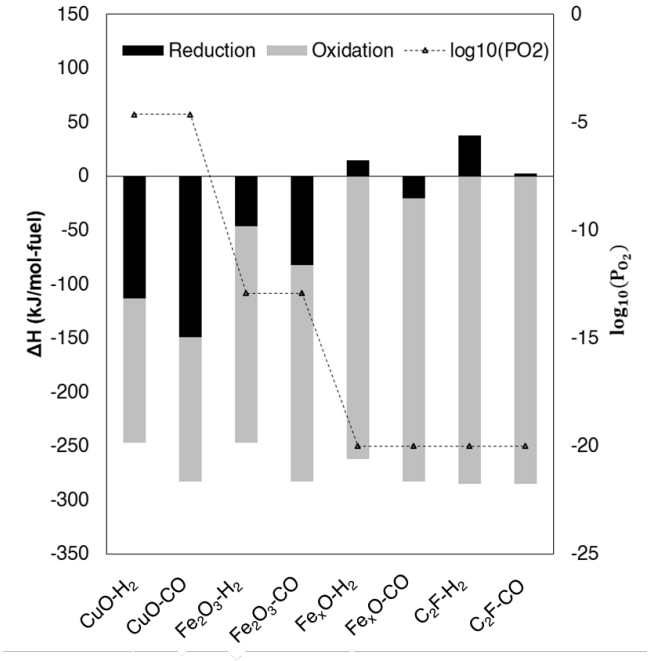
are related to ΔH_{O_2} by $\Delta H_{R-3} = \Delta H_{combust} + \Delta H_{O_2}$, where $\Delta H_{combust}$ is the standard heat of combustion in gaseous oxygen for either CO or H_2, giving

$$\Delta H_{R-3} = \Delta H_{combust} + T\Delta S_{O_2} - 0.5RT\ln(P_{O_2}) \qquad \textbf{(Eq. 2)}$$

Since ΔS_{O_2} is approximately constant for most oxygen carriers [34], the equilibrium P_{O_2} largely determines the value of ΔH_{O_2} and thus ΔH_{R-3}. Very low P_{O_2} oxygen carriers are needed to give endothermic conversion of CO or H_2. The value of P_{O_2} can be directly related

to the equilibrium P_{CO}/P_{CO_2} or P_{H_2}/P_{H_2O} at equilibrium, with a low value of P_{O_2} implying values of P_{CO}/P_{CO_2} or P_{H_2}/P_{H_2O} sufficiently large that the metal oxide reduction can be easily reversed with CO_2 or steam. Thus, suggesting oxygen carriers utilised in water-splitting processes [25,35–37] would be suitable candidates for the proposed application.

Fig. 2 illustrates that oxygen carriers with relatively high P_{O_2} phase transitions, such as CuO to Cu_2O ($\log_{10}(P_{O_2})$~ -5) and Fe_2O_3 to Fe_3O_4 ($\log_{10}(P_{O_2})$~ -13), respectively, are not suitable candidates since both exothermically oxidise H_2 and CO. The heat of combustion of the fuel (indicated by the total height of the bar) is split between the oxidation and reduction reactions. As P_{O_2} falls, more of the fuel's heat of combustion is released in the oxidation until very low values of P_{O_2} when the reduction becomes endothermic. For example, the wüstite (Fe_xO) to metallic Fe transition has $\log_{10}(P_{O_2}) = -20$ and $\Delta H^{\circ}_{R-3,650\,^{\circ}C}$ of 15 and -21 kJ/mol-fuel in H_2 and CO, respectively [33]. Iron oxides have been previously investigated in hydrogen production using steam; however, deep reduction of unsupported iron oxides leads to severe sintering, causing rapid deactivation after only a few redox cycles [38,39]. Therefore, supports are essential to maintain the iron oxide's performance over reasonable cycles. Inert supports do not form mixed phases, and therefore the iron oxide has the same phase transitions as pure iron oxide, for example, ZrO_2 [40] and $MgAl_2O_4$ [41]. Some support materials form mixed oxides or solid solution phases with the iron oxides and alter the equilibrium of the phase transitions, e.g., TiO_2 [42], Al_2O_3 [43], MgO [44,45], and CaO [24,25].



137

138 **Figure 2** Enthalpy of reaction for reduction and oxidation (per mole of fuel

139 combusted) for different redox reactions at ~650 °C, except for Fe_xO and C_2F at ~750 °C

140 using data from MTDATA [33].

141 The mixed oxides of calcium and iron have previously been suggested as looping

142 materials [24,25,36,37,46–48]. They are made up of abundant and cheap oxides and are already

143 used in the steel-making process, hence are the focus of this work. Dicalcium ferrite ($Ca_2Fe_2O_5$,

144 C_2F) has been widely investigated for chemical looping hydrogen production via water splitting

145 [25,35–37]. It is remarkably stable in cyclic reduction-oxidation processes [25,35,37,47] and

146 has roughly similar P_{O_2} for its reduction than wüstite, i.e., $\log_{10}(P_{O_2})$ of -20 [33], which

147 according to the well-known phase diagram, should occur as a single reaction to CaO and

148 metallic Fe [25,33,35], i.e.,

$$Ca_2Fe_2O_{5(s)} \leftrightharpoons 2CaO_{(s)} + 2Fe_{(s)} + {}^3/_2\, O_{2(g)} \qquad \textbf{(R-4)}$$

149 or with CO of H_2,

$$Ca_2Fe_2O_{5(s)} + 3CO_{(g)} \leftrightharpoons 2CaO_{(s)} + 2Fe_{(s)} + 3CO_{2(g)} \qquad \textbf{(R-5)}$$

$$Ca_2Fe_2O_{5(s)} + 3H_{2(g)} \leftrightharpoons 2CaO_{(s)} + 2Fe_{(s)} + 3H_2O_{(g)} \quad \textbf{(R-6)}.$$

150 The $\Delta H^{\circ}_{650\,^{\circ}C}$ for **R-5** and **R-6** are around 2 and 38 kJ/mol-fuel, respectively, as shown in **Fig.**
151 **2**, implying C_2F is a suitable oxide candidate. The P_{O_2} value can also be expressed as P_{CO}/P_{CO_2}
152 and P_{H_2}/P_{H_2O} for **R-5** and **R-6** with values of ~3.3 and ~3.8 at 780 °C, respectively [20,33].
153 C_2F alone would not be able to combust CO and H_2 completely. However, C_2F is also a
154 multifunctional material, releasing CaO as it reduces, which can carbonate and act as a CO_2
155 sink, i.e., a reductive-carbonation reaction. For example, combing **R-5** with **R-1** drives the
156 reaction to convert the CO, and depending on the partial pressure of CO_2, and the ratio of CO
157 to CO_2, allows other iron oxides to form, for example,

$$Ca_2Fe_2O_{5(s)} + 3CO_{(g)} \leftrightharpoons 2CaCO_{3(s)} + 2Fe_{(s)} + CO_{2(g)} \quad \textbf{(R-7)}.$$

158 Equally on the regeneration, the oxidative-calcination can occur; the formation of C_2F makes
159 it easier to release the CO_2, and oxidise the Fe^0 to Fe^{3+}. This, of course, is driven by the fact
160 C_2F is a mixed phase with a lower free energy than equivalent amounts of Fe_2O_3 and CaO, e.g.,

$$2Fe_{(s)} + 2CaCO_{3(s)} + 1.5O_{2(g)} \rightleftharpoons Ca_2Fe_2O_{5(s)} + 2CO_{2(g)} \quad \textbf{(R-8)}.$$

161 The CaO can be sourced either from the reduced phases of the C_2F (CaO+Fe), by adding excess
162 CaO onto the C_2F as a composite particle, or by feeding separate CaO particles to the system.

163 Different compositions of CaO and Fe_2O_3 would lead to different phases formed in the
164 Fe – Ca – O system. When a limited amount of CaO is available, a mixture of Fe_2O_3 and/or
165 $CaFe_2O_4$ forms. C_2F is the only mixed oxide that should form if Fe/(Ca+Fe) < 0.5, i.e., with
166 excess CaO the solid looping material should consist of C_2F and CaO (i.e., C_2F/CaO) [35]. In
167 this work Fe/(Ca+Fe) ≤ 0.5 is utilised, since CaO is needed to capture the CO_2. C_2F
168 performance in combusting various fuels, e.g., CO [25,35], CH_4 [49,50], and H_2 [49] has been
169 previously evaluated, but mainly at higher temperatures (> 800 °C) when carbonation of CaO

would not occur at atmospheric pressure. Sufficiently low temperatures, ~600 °C, are necessary to allow carbonation instead of direct reincorporation into C_2F [25].

In this work, using C_2F as a chemical heat pump in **Fig. 1** is demonstrated in a thermogravimetric analyser and a fluidised bed. Here, lower temperatures are investigated since carbonation is required to treat BFG. C_2F, C_2F/CaO composites, and C_2F and CaO as separate particles in a fluidised bed are evaluated for reductive-carbonation using hypothetical BFG with a ratio P_{CO}/P_{CO_2} of ~1.3 over cycles which mimic the process shown in **Fig. 1**.

2. Materials and methods

2.1. Materials characterisation

Materials were characterised using X-ray diffraction (XRD) analysis (Siemens D500 x-ray diffractometer, Cu Kα radiation; operated at 35 kV and 20 mA; a scan range between 5° and 90° in 2θ with a step size of 0.02°. The materials were tested on an aluminium mount.

2.2. Materials synthesis

To prepare C_2F and C_2F/CaO composite, Fe_2O_3 (Iron (III) oxide, 98%, Thermo fisher scientific) and $CaCO_3$ (calcium carbonate precipitated, Fisher Scientific) were ball milled at 30 Hz for 3 hours to give a mole ratio of Fe/(Fe+Ca) of 0.5 and 0.3. 10 %wt potato starch (BDH Laboratory Supplies) was added to improve microstructure and deionised (DI) water was used to improve the mixing in the ball mill. The homogenous slurry was then dried overnight in the oven at 100 °C, before finally calcined in the furnace for 6 hours at 1000 °C, and crushed into desired particle size, i.e., 355 – 500 μm for experiments in a thermogravimetric analyser (TGA) and 500 – 1000 μm in a fluidised bed. The mixing, drying, and calcination were repeated once for the C_2F/CaO composite to improve its hardness and prevent severe attrition in the fluidised bed. C_2F alone was formed when Fe/(Fe+Ca) in the precursors is exactly 0.5, as seen in XRD patterns in **Fig. 3.** As expected, the composite comprised a mixture of 'free' CaO and C_2F [35].

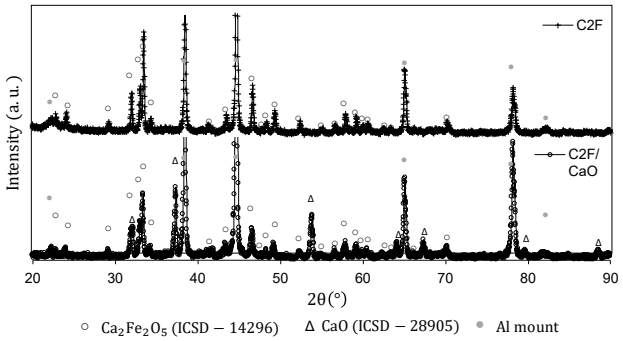


Figure 3 XRD pattern of as-prepared C_2F and C_2F/CaO. The obtained diffractograms were then compared with reference patterns from the Inorganic Crystal Structure Database (ICSD), i.e., ICSD – 14296 for $Ca_2Fe_2O_5$ and ICSD – 28905 for CaO.

2.3. Thermogravimetric analysis

The thermogravimetric analyser (TGA, Mettler – Toledo TGA/DSC 1) comprised a microbalance equipped with an electrically-heated horizontal tube furnace on which an alumina crucible was placed. Typically, the TGA chamber was constantly purged with N_2 as protective and purging gases with 50 mL/min (20 °C, 1 atm) each, unless stated otherwise. Reactive gas, typically at 50 mL/min (20 °C, 1 atm) was fed to the system via a capillary tube above the crucible.

The material's ability to transfer its lattice oxygen and capture CO_2 was studied in the TGA. The sample was (i) reduced in CO/N_2 for 150 mins, (ii) carbonated in CO_2 for 120 mins, (iii) oxidised in a mixture of CO_2 and air at isothermal temperatures of 650 and 700 °C, before finally (iv) heated up from isothermal temperatures to 900 °C at 5 °C/min and (v) further oxidised for 30 mins at 900 °C in air/CO_2. To examine CO_2 capture alone in a carbonation and calcination cycle, typically, a sample was reacted in CO_2 at a constant temperature of 650 °C for 120 mins and followed by the calcination by ramping the temperature to 900 °C at 20

°C/min under CO_2. Limestone (425 – 600 μm, its XRD result is given in **Fig. S1**, labelled as "Limestone A") was also tested for calibration and comparison. Before actual experiments, as-synthesised materials and limestone were dried by ramping temperature from ambient to 900 °C at 20 °C/min and holding it isothermally in air for 30 mins so all materials were in their calcined states.

2.4. C_2F and C_2F/CaO composite performance in treating a hypothetical blast furnace gas in a fluidised bed

As-prepared materials, i.e., C_2F and C_2F/CaO composite were reacted with a hypothetical blast furnace gas (BFG) in a fluidised bed (described in detail elsewhere [47]). The hypothetical BFG comprised CO and CO_2 with a ratio of P_{CO}/P_{CO_2} is around 1.3. For comparison, a mixture of separate particles of C_2F and limestone (600 – 1000 μm, its XRD result is given in **Fig. S1**, labelled as "Limestone B"), referred to as C_2F+limestone, was tested, with an overall Fe/(Fe+Ca) ratio the same as the C_2F/CaO composite.

A typical cycle was performed by feeding 7 g of as-prepared materials into a preheated bed filled with alumina sand (~30 g, Boud Minerals, grade FEPA-46, size 350 – 420 μm) under N_2 at 900 °C to remove all the absorbed moisture and CO_2. The reactor was then cooled to 650 °C in N_2 and followed by (i) reacting the materials with hypothetical BFG (7% CO_2/9.3% CO balance with N_2) for 30 mins (reductive-carbonation), (ii) purging under N_2 for 20 mins while ramping the reactor temperature from 650 to 800 °C at a rate of ~30 °C/min (purging), (iii) oxidation in 20%CO_2/N_2 for 5 min and (iv) in air for 5 min at 800 °C. This cycle was repeated at least three times for every prepared material. All the gases were supplied from gas cylinders (BOC) of 10% CO/N_2, 100% CO_2, compressed air, and N_2 with a total flow rate of ~33 mL s^{-} at NTP (20 °C, 1 atm) for C_2F and C_2F/CaO composite, and ~25 mL s^{-} at NTP (20 °C, 1 atm) for C_2F+limestone. The gaseous products were pumped (16 mL s^{-}) to be analysed using gas

238 analysers (ABB EL3020) equipped with a non-dispersive infrared (NDIR, ABB Uras26) cell
239 for CO and CO_2 . To summarise, **Table 1** shows as-prepared materials studied in the fluidised
240 bed.

241 **Table 1**. As-prepared materials studied in the fluidised bed.

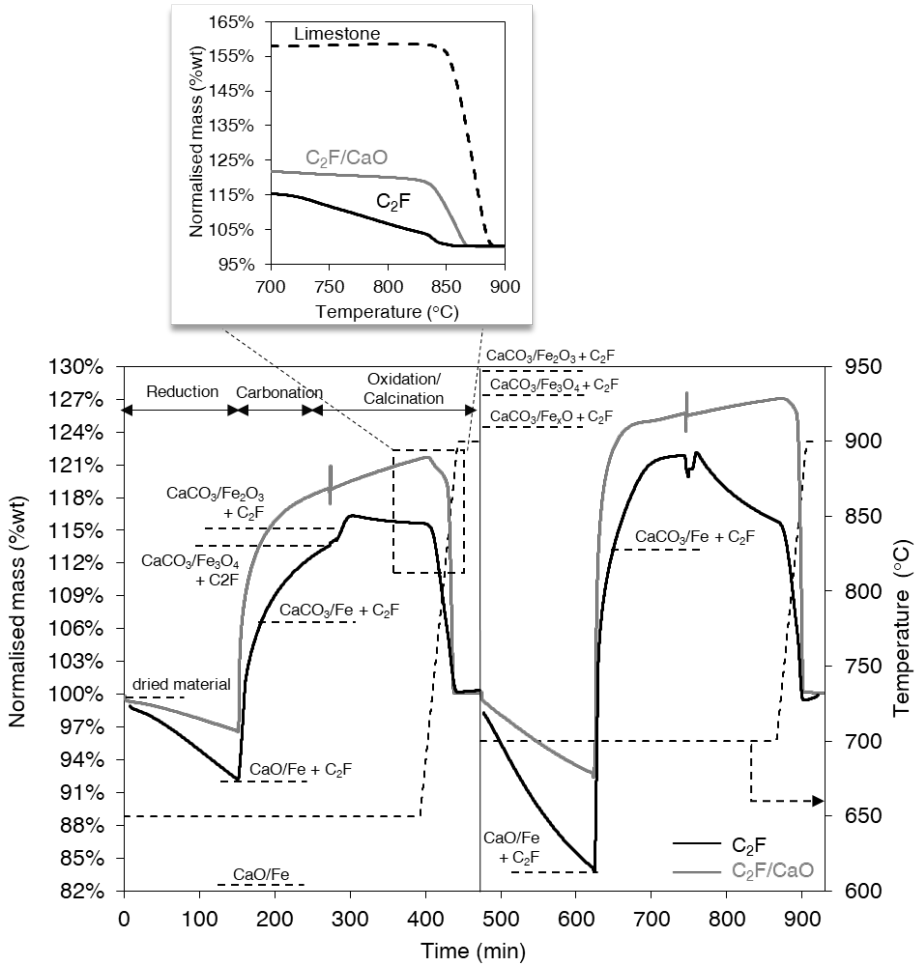
Notation	OCs	CO_2 sorbent	Fe/(Fe+Ca)
C_2F	$Ca_2Fe_2O_5$	N/A	0.5
C_2F/CaO	$Ca_2Fe_2O_5$	CaO	0.3
C_2F+limestone	$Ca_2Fe_2O_5$	Calcined limestone	0.3

242

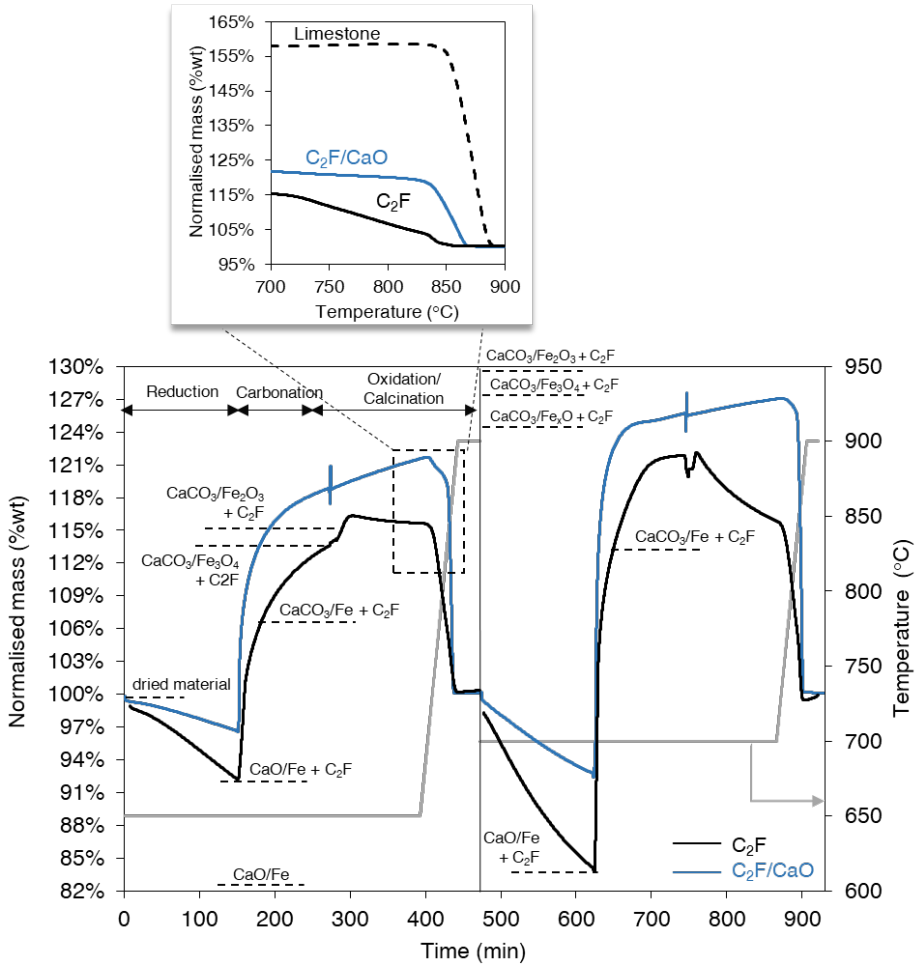
243 **3. Results**

244 *3.1 Reduction – carbonation – oxidative calcination in the TGA*

245 The ability of the C_2F and the C_2F/CaO composite to transfer their lattice oxygen and
246 capture CO_2 in reduction, carbonation, oxidation, and calcination in CO_2/air is shown in **Fig.**
247 **4**. The fresh C_2F was not fully reduced in CO at 650 °C in the time allowed, giving up only
248 ~0.08 g-oxygen/g-C_2F (~45% C_2F conversion), leaving a mixture of CaO/Fe and C_2F. When
249 all the CaO formed during reduction is carbonated to $CaCO_3$, the mass gain should be 14.7wt%,
250 giving a normalised mass of around 106.7wt% (see **Fig. 4**). However, the final mass at the end
251 of carbonation reached ~114wt%, indicating that oxidation also occurred, consistent with all
252 the formed CaO and metallic Fe being converted to $CaCO_3$ + Fe_3O_4 (21.8wt% gain, reaching
253 a mass of ~114wt% in **Fig. 4**). This agrees with the behaviour expected from the
254 thermodynamics of the Fe – Ca – O system (**Fig. 5**). Carbonation with P_{CO_2}= 0.34 atm should
255 convert the Fe to Fe_3O_4 and $CaCO_3$ at 650 °C as shown in **Fig. 5**, with the extent of oxidation
256 beyond Fe_3O_4 limited by equilibrium P_{CO}/P_{CO_2} produced by the oxidation reaction.


Limestone
C2F/CaO
C2F
Normalised mass (%wt)
Temperature (°C)
Reduction
Carbonation
Oxidation/
Calcination
CaCO3/Fe2O3 + C2F
CaCO3/Fe3O4 + C2F
CaCO3/FexO + C2F
CaCO3/Fe2O3
+ C2F
CaCO3/Fe3O4
+ C2F
CaCO3/Fe + C2F
dried material
CaO/Fe + C2F
CaO/Fe
CaO/Fe
+ C2F
C2F
C2F/CaO
Normalised mass (%wt)
Temperature (°C)
Time (min)

257



258

259 **Figure 4** Normalised mass in %wt vs time of C_2F (—) vs C_2F/CaO (—) in the TGA. The
260 cycles comprise of (i) CO reduction for 150 mins, (ii) carbonation in CO_2 for 120 mins, (iii)
261 oxidation/calcination in air/CO_2 for 120 mins at temperatures of 650 and 700 °C and, (iv)
262 ramping up temperature to 900 °C at 5 °C/min, and (v) holding temperature at 900 °C in
263 air/CO_2 for 30 mins.

264 The unconverted C_2F is stable when exposed to CO_2. The subsequent
265 oxidation/calcination at 650 °C in a mixture of air and CO_2 (P_{CO_2} of ~0.25 atm) allowed further
266 oxidation with a mass gain of 0.9wt%, reaching ~116wt% consistent with all the Fe and CaO
267 produced on reduction being oxidised and carbonated to Fe_2O_3 + $CaCO_3$. The loss in mass then
268 started as the temperature was ramped from 650 to 900 °C in air/CO_2. At the end of each cycle,
269 the sample was able to attain its initial dried mass, i.e., complete calcination and oxidation

(labelled as dried material in **Fig. 4**). Assuming all the mass loss during temperature ramp-up in air/CO_2 was caused by decarbonation, the sample had a CO_2 capture capacity of ~0.15 g-CO_2/g-oxide. In the subsequent cycle at the higher temperature (700 °C) in the TGA (**Fig. 4**), the C_2F reached a higher conversion at the end of reduction, i.e., ~91%, releasing more CaO. The final mass after carbonation was ~122wt%, which is higher than expected if the converted material was only carbonated into Fe+$CaCO_3$ (i.e., 113.3wt%), but lower than expected if all metallic iron produced was oxidised either to Fe_xO (124.6wt%) or Fe_3O_4 (127.6wt%).

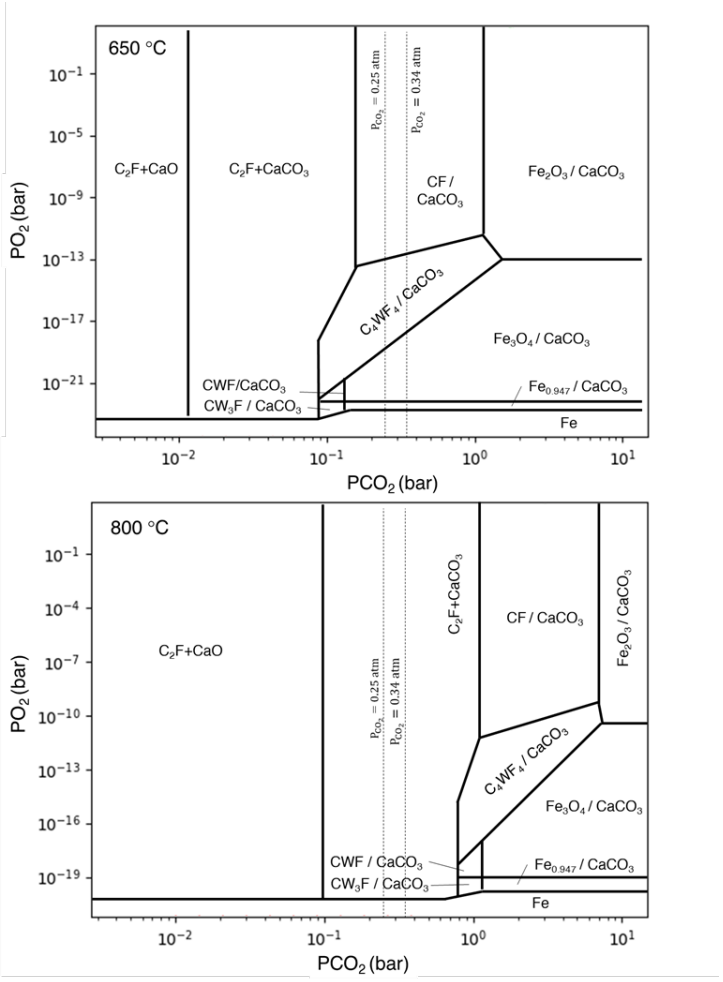


Figure 5 Predominance diagram of Fe – Ca – O system with Fe:Ca of 2:2.1 at 650 and 800 °C (computed using MTDATA [33], SUB-SGTE database for CO_2 and $CaCO_3$, and HTOX for all other species) [33].

The cycle of reduction – carbonation – oxidation/calcination was repeated in the fluidised bed so that sufficient material could be retrieved for XRD analysis (**Fig. 6**). The as-synthesised C_2F (**Fig. 6A**) was reacted with 10%CO/N_2 for 30 mins and then exposed in CO_2 for 30 mins at 650 °C (**Fig. 6B)**. The XRD patterns in **Fig. 6B** shows that a mixture of $CaCO_3$+Fe_3O_4+Fe_xO was formed and no C_2F peaks were observed. Fe_xO presumably had not finished oxidising into Fe_3O_4. When the reduced C_2F was reacted in CO_2 and then exposed to a mixture of 20%CO_2/air for 5 mins at 650 °C (**Fig. 6C**), $CaCO_3$, Fe_xO, and Fe_3O_4 peaks were still observed, and as the reaction was prolonged up to 15 mins (**Fig. 6D**), C_2F started to form, though the $CaCO_3$, Fe_3O_4, and Fe_xO peaks were still observed.

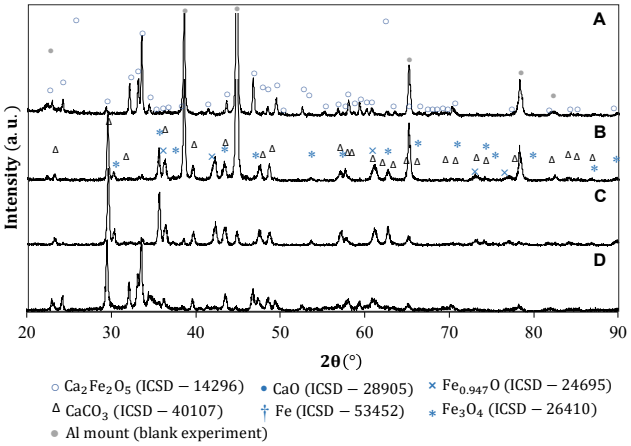


Figure 6 XRD patterns of C_2F as prepared [**A**], C_2F after reduction in 10%CO/N_2 for 30 mins and carbonation in 20%CO_2/N_2 for 30 mins [**B**], and C_2F after reduction in 10%CO/N_2 for 30 mins, carbonation in CO_2/N_2 for 30 mins and oxidation in 20%CO_2/air for 5 mins [**C**] or 15 mins [**D**] at 650 °C. The obtained diffractograms were then compared with reference patterns from the Inorganic Crystal Structure Database (ICSD), i.e., ICSD – 14296 for $Ca_2Fe_2O_5$, ICSD – 40107 for $CaCO_3$, ICSD – 28905 for CaO, ICSD – 15840 for Fe_2O_3, ICSD – 26410 for Fe_3O_4, ICSD – 24695 for $Fe_{0.947}O$, and ICSD – 53452 for Fe.

Reduction in CO for an extended reaction time (180 mins) at 650 °C to increase the C_2F conversion and CaO availability, carbonation in CO_2 (P_{CO_2} = ~0.34 atm) at 650 °C for 120 mins,

and oxidation by ramping up the temperature to 900 °C at a rate of 10°C/min in CO_2/air (P_{CO_2}= ~0.25 atm) were repeated for consecutive cycles as shown in **Fig. 7**. The oxygen transfer capacity and CO_2 capture capacity of C_2F through 15 cycles appeared to be relatively stable of ~0.1 g-oxygen/g-material and ~0.2 g-CO_2/g-material, respectively for the given time. The theoretical oxygen transfer capacity of C_2F is 0.177 g-oxygen/g-C_2F, while its fully-reduced form should be able to capture 0.324-CO_2/g-C_2F.

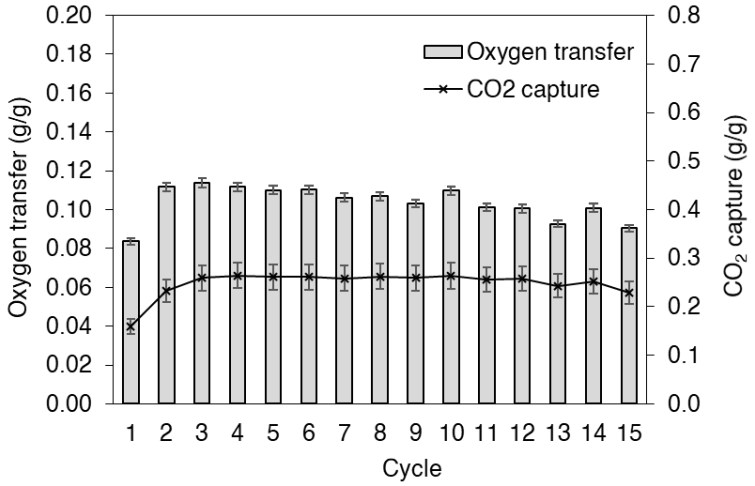


Figure 7 Cyclic reduction – carbonation – oxidative/calcination of C_2F in the TGA. The error (depicted as error bars here) was estimated by comparing mean values of oxygen transfer and CO_2 capture capacity from this experiment (in **Fig. 7**) and repeated similar cycles for 10 times (not shown).

Cyclic carbonation and calcination of the C_2F/CaO composite were performed by reacting the composite with CO_2 at 650 °C and then within the same atmosphere ramping the temperature from 650 to 900 °C at a rate of 10 °C/min to drive calcination. **Fig. 8A** shows that the fully-oxidised composite had a relatively stable CO_2 uptake throughout 10 cycles (i.e., 0.1 g-CO_2/g-composite). When the composite was initially reduced under CO with similar cycles as for C_2F in **Fig. 7**, the CO_2 capture capacity was initially ~0.15 g-CO_2/g-composite, and increasing as the cycle continued to finally reach ~0.3 g-CO_2/g-composite after 10 cycles (**Fig.**

8A and S20). Though there was extra CaO available in the reduced form of the composite, this only added an additional 0.055 g-CO_2/g-composite of CO_2 absorption capacity (from 0.03 g-oxygen/g or 30% conversion of the composite). The greater CO_2 capacity in cyclically reduced composite is likely caused by a greater accessibility of CaO as the material is cycled. In comparison, fresh limestone and sintered $CaCO_3$ powder (Fisher Scientific, sintered for 6 hours at 1000 °C) in their calcined states, initially showed a higher CO_2 capture capacity, i.e., 0.6 and 0.4 g-CO_2/g-material at cycle 1, respectively, and declined to 0.26 and 0.34 g-CO_2/g-material at cycle 10 (**Fig. 8A**).

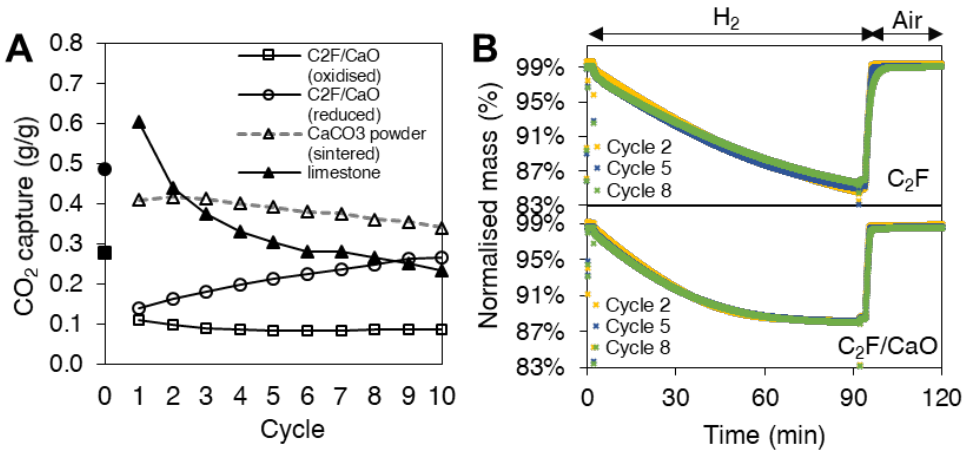


Figure 8 [**A**] CO_2 capacity in grams of CO_2 per gram of materials vs number of cycles of (—□—) fully oxidised C_2F/CaO composite, (—○—) partially reduced C_2F/CaO composite, (--Δ--) sintered $CaCO_3$ powders, and (—▲—) calcined limestone during 2 hours carbonation under CO_2. ● is theoretical CO_2 capture capacity if the C_2F/CaO is fully reduced into CaO+Fe and all CaO is carbonated; and ■ theoretical CO_2 capture capacity of a fully oxidised composite; [**B**] isothermal redox cyclic experiment in the TGA at 900 °C of C_2F and C_2F/CaO composite in H_2 for 90 mins, and oxidation in air for 30 mins. The mass was normalised from the mass of dried materials after drying in air at 900 °C for 30 mins.

335 Cyclic reduction of materials was also tested by reacting C_2F and C_2F/CaO in H_2 for 90
336 mins at 900 °C and reoxidation was performed in air. The C_2F/CaO was able to reversibly
337 transfer its oxygen lattice and reached its maximum oxygen transfer capacity, i.e., ~0.11 g-
338 oxygen/g-material (**Fig. 8B**). C_2F had an oxygen transfer capacity of 0.143 g-oxygen/g-
339 material, and did not reach its maximum capacity (~0.177 g/g) in the time allowed. Longer
340 reduction should have completely reduced the C_2F [24].

341 *3.2 Performance of C_2F, C_2F/CaO composite and separate particles of C_2F and calcined*
342 *limestone (C_2F+limestone) in the fluidised bed*

343 When the C_2F was exposed to hypothetical BFG (P_{CO}/P_{CO_2}= 1.3) at 650 °C, there was a
344 peak in the consumption of CO_2 at the beginning in **Fig. 9A(i)**, indicating some oxidation of
345 CO to CO_2 with a maximum CO conversion of ~20% at ~2 min. Some CO and CO_2 was
346 produced during purging in N_2 (**Fig. 9A(ii))** (ramping the temperature from 650 to 800 °C at
347 ~30°C/min), indicating that absorbed CO_2 is able to reoxidise some of the reduced C_2F. The
348 solid was then reoxidised in 20% CO_2/N_2 at 800 °C CO_2, producing CO (**Fig. 9A(iii))** before
349 final oxidation in air to ensure complete oxidation (not shown). Around 40% of the CO was
350 produced during purging from the absorbed CO_2, while the remaining was generated during
351 CO_2 oxidation.

352 The C_2F/CaO composite also consumed both CO and CO_2 with a maximum CO
353 conversion of ~25% at t = ~2 min (**Fig. 9B(i)**) during reductive-carbonation at 650 °C.
354 P_{CO}/P_{CO_2} remained at ~3 until about t = 3 min before dropping to 1.5, then at t > 15 min
355 reaching the inlet P_{CO}/P_{CO_2} of 1.3. During the purging step (**Fig. 9B(ii)**), both CO and CO_2
356 were generated and much less CO was generated during CO_2 oxidation step, i.e., only 5% of
357 the total produced CO (**Fig. 9B(iii)**). This means that extra CaO in the C_2F/CaO composite was

able to capture enough CO_2 during reductive-carbonation step to self-oxidise the reduced C_2F during purging step.

The composite was able to capture ~0.2 g-CO_2/g-composite during the reductive-carbonation step in the fluidised bed (**Fig. 9B(i)**), which is relatively close to the theoretical CO_2 capacity of the fully-oxidised composite (i.e., 0.278 g-CO_2/g-composite). If the composite is fully reduced (i.e., CaO+Fe), its maximum CO_2 capture capacity becomes 0.487 g-CO_2/g-composite. Separate particles of C_2F and calcined limestone (C_2F+limestone) with the similar Fe/(Fe+Ca) ratio as the C_2F/CaO composite, i.e., 0.3, behaved similarly to the C_2F/CaO with P_{CO}/P_{CO_2} of ~3 before approaching the P_{CO}/P_{CO_2} of ~1.3 after 10 mins (**Fig. S2(i)**).

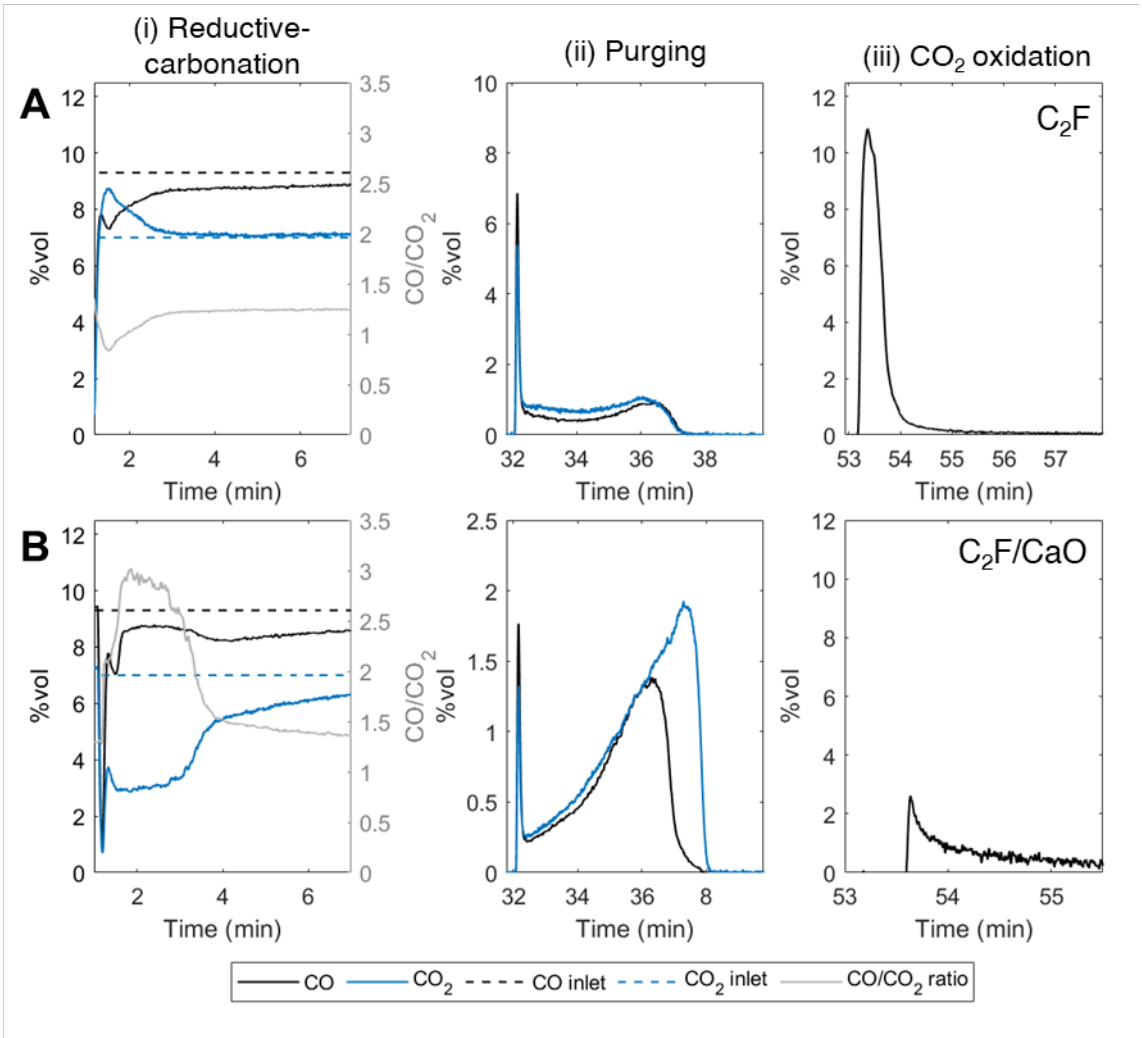


Figure 9 Profile of off-gas concentration during cyclic experiment comprised of (i) reductive-carbonation in the hypothetical BFG at 650 °C, (ii) purging in N_2 by ramping up the temperature to 800 °C at 30 °C/min, and (iii) oxidation in CO_2 at 800 °C of C_2F [**A**] and C_2F/CaO composite [**B**].

The total CO_2 absorbed during the reductive-carbonation step was estimated from the amount of CO and CO_2 released during the purging step, whilst the total oxygen released from the material was calculated from the CO generated during the purge and CO_2 oxidation. Carbon removal was calculated based on total CO consumed and CO_2 capture during reductive-carbonation step as carbon equivalent in gram. The C_2F/CaO composite and C_2F+limestone were able to capture 0.2 and 0.09 g-CO_2/g-material and release 0.06 and 0.014 g-O/g-C_2F on average over three cycles (**Fig. 10)**, while the C_2F captured ~0.04 g-CO_2/g-material and released 0.016 g-O/g-C_2F. Accordingly, total carbon removal (CO+CO_2) of the C_2F, C_2F/CaO composite, and C_2F+limestone was 0.018, 0.055, and 0.024 g-carbon/g-material, respectively.

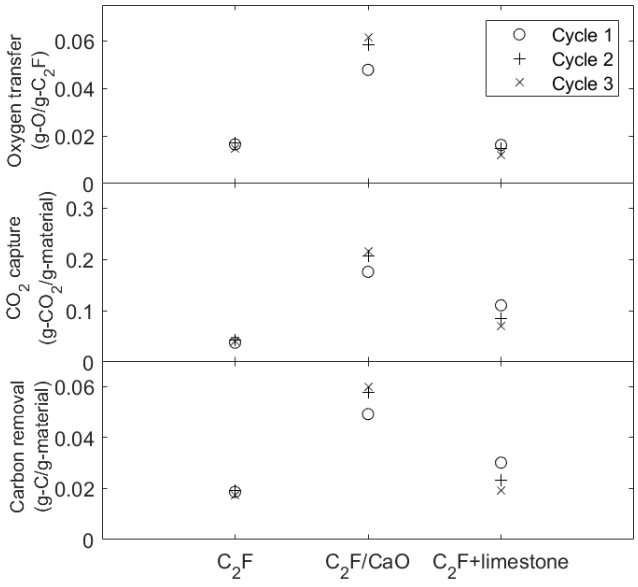


Figure 10 Oxygen transfer capacity, CO_2 capture and total carbon removal of C_2F, C_2F/CaO composite and separate C_2F+limestone during reductive-carbonation using hypothetical BFG in the fluidised bed for three times repetitive cycles.

4. Discussion

The normalised mass profile during carbonation both at 650 and 700 °C in **Fig. 4** demonstrates the typical carbonation profile for CaO which comprised of (i) an initial kinetically limited regime which is commonly distinguished by a fast carbonation profile in the beginning of carbonation step, and followed by (ii) a slower regime which is diffusion limited [15,30]. When C_2F was initially reduced in CO and then exposed to CO_2 (P_{CO_2}= 0.34 atm) in the TGA at 650 °C in **Fig. 4**, it obtained a final mass of ~114wt%, indicating that the material is carbonated as well as oxidised to reach a mixture of $CaCO_3$ + Fe_3O_4, which corresponds to the phases expected from **Fig. 5**. Interestingly, **Fig. 5** suggests that further oxidation of $CaCO_3$ + Fe_3O_4 in air/CO_2 (P_{CO_2}= 0.25 atm) should have converted the materials into CF + $CaCO_3$. However, instead of losing mass due to $CaCO_3$ decomposition, the material gained a little mass, reaching the level as if Fe_3O_4 is further oxidised into Fe_2O_3 (i.e., ~116wt%). It seems that there is a kinetic effect on the decomposition and incorporation of $CaCO_3$ + Fe_3O_4 into CF + $CaCO_3$. The oxidation of Fe_3O_4 to Fe_2O_3 appears to be faster, resulting a mixture of C_2F + Fe_2O_3 + $CaCO_3$.

At 700 °C and the same P_{CO_2} during carbonation (P_{CO_2}= 0.34 atm), the material should have seen conditions where more complicated ferrites can form (see **Fig. S6**). If one of these ferrites form e.g., CW_3F+$CaCO_3$, CWF+$CaCO_3$, or C_4WF_4+$CaCO_3$, the final mass should have been ~120, 117.8, and 115.7wt%, respectively which was lower than the final mass gain after it was exposed to CO_2 in **Fig. 4** (~122wt%). The material also did not reach its theoretical mass if all CaO and Fe were converted into $CaCO_3$ + Fe_xO (124.6wt%). There could be a competition between carbonation of CaO → $CaCO_3$ vs oxidation and formation of ferrites. In fact, at 700 °C, the kinetics of carbonation of reduced C_2F under CO_2 is much faster than the oxidation [37]. As the material was reacted with a mixture of air/CO still at 700 °C, the mass dropped

409 and reached 115.8 wt% which is roughly the mass expected for the C_4WF_4+$CaCO_3$ (i.e., 115.7
410 wt%) or CF+$CaCO_3$ (i.e., 114.7 wt%). Although, CF is likely to form when the material was
411 exposed in air, there might be the kinetic limitations as well.

412 Since C_2F is a mixed phase (with a lower free energy), it is relatively stable compared to
413 its separate components, i.e., CaO and Fe_2O_3. Employing a mixed phase, such as C_2F in its
414 reduced form as CaO + Fe to capture CO_2 forming $CaCO_3$, allows P_{CO_2} for decarbonation to
415 be lowered, depending on the P_{O_2} during calcination, i.e., decarbonation in Fe – Ca – O system
416 can be driven by the reincorporation of the calcium oxide into C_2F. Whilst pure $CaCO_3$ is
417 expected to decarbonate at ~890 °C ($P_{CO_2} = 1$ bar) [20], the reduced-carbonated Fe – Ca – O
418 phases (e.g., $CaCO_3$+Fe_3O_4) would decarbonate at temperatures as low as 750 °C [33]. **Fig. 4**
419 shows that the $CaCO_3$+Fe_3O_4 started to decarbonate at ~695 °C. At similar conditions ($P_{CO_2} =$
420 0.25 atm), limestone started to calcine at ~845 °C in the TGA. A lower temperature gap
421 between carbonation and calcination steps means less energy is needed to complete the cycle.

422 Gu et al. [51] observed the similar phenomenon in using SrO as a CO_2 sorbent within Ce
423 – Sr – O system. $SrCO_3$ should have decomposed at ~1225 °C when P_{CO_2} = 1 bar [20] if the
424 decarbonation occurs via $SrCO_3$ → SrO + CO_2, but instead decomposed at ~850 °C. The lower
425 decarbonation temperature was caused by the formation of Sr_2CeO_4, i.e., $SrCO_3$ + CeO_2 →
426 Sr_2CeO_4. Lowering decarbonation temperature would not only benefit the energy requirement
427 for the calciner, but also might minimise the sintering problem which is the typical issue for
428 the CaL [52–54] since Tamman temperature of $CaCO_3$ is 533 °C, whilst 1154 °C for CaO. It is
429 important to note that not all mixed phases would be as stable as the C_2F, significantly lowering
430 the P_{CO_2} for decomposition. In the typical copper-calcium looping [29], for example, formation
431 of mixed phases of Ca – Cu – O system does not significantly shift the P_{CO_2} for calcium
432 carbonate decomposition, although the mixed phases still have a lower free energy than their

433 separate oxides, the difference is not sufficient to significantly alter the decarbonation
434 temperature [17].

435 Turning to the results from the fluidised bed in **Fig. 9**, C_2F should not combust the
436 hypothetical BFG, given its P_{CO}/P_{CO_2} = 1.3 is less than the equilibrium P_{CO}/P_{CO_2} ~3 for C_2F
437 reduction in **R-5**. Other iron containing phases are one explanation. The presence of iron-
438 containing oxides other than C_2F would imply free CaO (undetected by XRD in **Fig. 3**). To test
439 the presence of free CaO, the C_2F was reacted under CO_2 from 200 – 900 °C at 2 °C/min (see
440 **Fig. S7**) and there was very little mass gained (0.3wt%) during carbonation, which would imply
441 only ~0.0038 g-CaO/g-C_2F. This implies 0.0054 g-Fe_2O_3/g-C_2F or 0.0052 g-Fe_3O_4/g-C_2F as
442 the impurity. If the CO combustion in **Fig. 9A** came from these impurities, the maximum
443 oxygen transfer should have been 0.00164 and 0.00145 g-O/g-C_2F, respectively, much less
444 than then observed oxygen transfer, 0.016 g-O/g-C_2F in **Figs. 9A** and **10**.

445 If either Fe_2O_3 or Fe_3O_4 significantly contributes to the oxygen transfer during reductive-
446 carbonation at 650 °C in **Fig. 9**, it should also do so at a higher temperature e.g., 750 °C (see
447 **Fig. S8**), when carbonation cannot occur. The P_{CO_2} of $CaCO_3$ → $CaO + CO_2$ is 0.1 bar at 750
448 °C [20], indicating CaO should not be able to absorb CO_2 in the hypothetical BFG (P_{CO_2} =
449 0.07 bar). Additionally, P_{CO}/P_{CO_2} for Fe_2O_3 → Fe_3O_4, Fe_3O_4 → Fe_xO, and Fe_xO → Fe are
450 0.00002, 0.42, and 1.6 at 750 °C, respectively [33], suggesting Fe_2O_3 or Fe_3O_4 should be able
451 to react with CO in the hypothetical BFG. Thus, the small amount of reduction observed in in
452 **Fig. S8** is likely caused by the reduction of phase impurities (like Fe_2O_3), and these phase
453 impurities result in only a small oxygen transfer, i.e., only ~ 10% of the total observed oxygen
454 transfer during reductive-carbonation of the C_2F (in **Fig. 9A**) when carbonation is possible. In
455 order for the bulk phase C_2F to react with BFG, the temperature must be low enough to also
456 ensure carbonation is possible.

To investigate further, the C_2F and C_2F/CaO composite were reacted with a mixture of CO and CO_2 in the TGA (see **Fig. 11**). For this experiment, only 15 mL/min protective gas (without purging gas) was fed to the TGA to lower the dilution effect. CO and CO_2 were set (i.e., 9.3 and 7.3%vol, respectively) to give P_{CO}/P_{CO_2} of 1.3; if the reactions gases mixed fully with the protective gas the CO and CO_2 would have been diluted to 7.1 and 5.6%vol, respectively. For the C_2F, mass began to increase (indicating carbonation) at 505 °C as shown from the DTG curve in **Fig. 11A**, reaching ~104 wt% of its dried mass, before finally dropping (i.e., calcination) back to the initial mass at 655 °C. For comparison, with the calcined limestone (CaO) in **Fig. 11C**, the limestone (as $CaCO_3$) started to lose mass at 765 °C as shown in DTG curve in **Fig. 11C**.

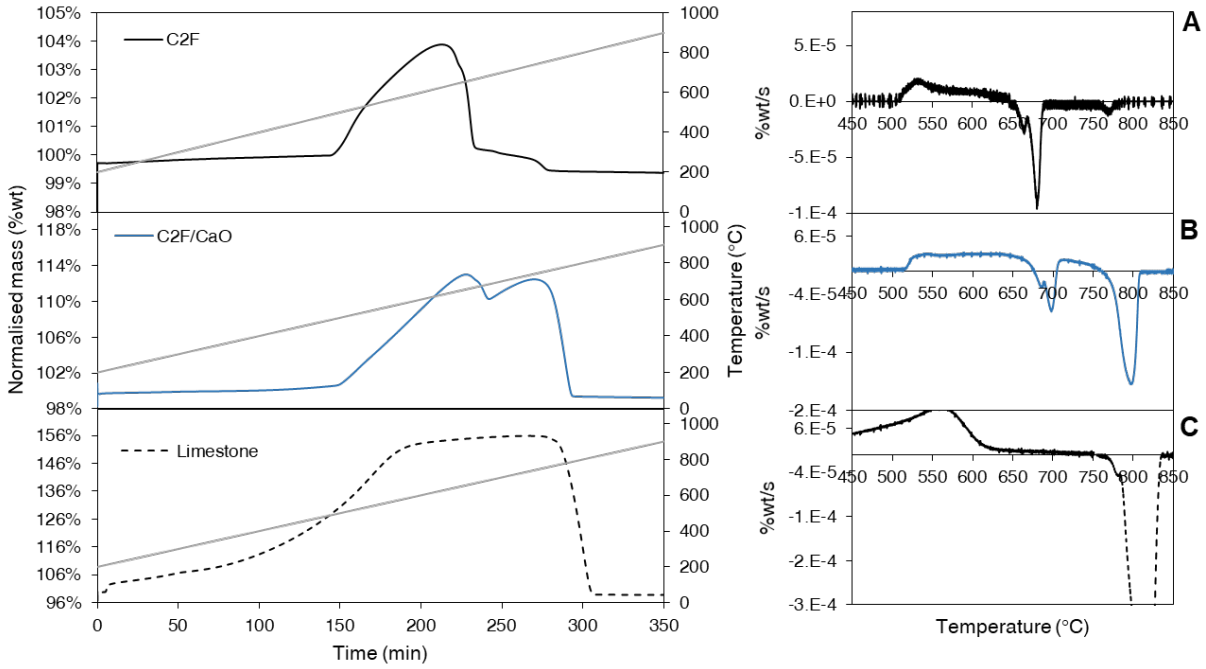


Figure 11 Temperature-programmed from 200 – 900 °C in a mixture of CO/CO_2 with a ratio of 1.3 at a rate of 2 °C/min in the TGA of [**A**] C_2F (—), [**B**] C_2F/CaO composite (—), and [**C**] calcined limestone (---). Initially, all materials are calcined in air for 30 mins at 900 °C.

Gas mixing in the TGA introduces uncertainty in the concentration seen by the sample. Here, this was minimised by lowering purge gas flow, constraining the CO_2 concentration to be between 5.6% (full mixing) and 7% (no mixing). This does not affect the ratio of CO to CO_2, but will have an impact on the carbonation reaction whose equilibrium is determined by the absolute CO_2 partial pressure. At a CO_2 concentration of 5.6%, limestone should have released its CO_2 at 717 – 724 °C, whilst at inlet concentration (7%), the decomposition temperature is 732 – 735 °C, depending on which data source is used for the thermodynamic equilibrium constant [33,34,55]. Calibration of sample temperature and thermal lag can also be an issue. Calibration using Zn melting point, 419.5 °C, gave 432 °C, suggesting a calibration lag error of 12.5 °C (**Fig. S10**). Repeating experiment in **Fig. 11** with different mass (see **Figs. S11** and **S12** for C_2F and limestone, respectively) showed onset temperatures for calcination were very similar, but once reaction has initiated larger initial masses resulted in more lag in mass loss. This indicates similar thermal lag for all experiments when heating, but significant heat or transport limitation once reaction is underway. Thus, the small difference between the observed and thermodynamically predicted decomposition can therefore be partly attributed to thermal lag in sample temperature and also kinetic effects.

After the sample lost almost all of its mass gain as shown in **Figs. 11 and S11**, there was a subsequent small mass loss at the temperature at which limestone decomposes. The mass losses were approximately 0.3wt%, regardless of total mass of samples, and is consistent with the amount of impurities detected in **Fig. S7**. At the end of TPR in the CO/CO_2 mixture in **Fig. S11**, any free iron oxide phase impurity would have been reduced to Fe, which would result in a final mass were slightly lower than the initial mass.

When the C_2F/CaO composite was reacted with the CO/CO_2 mixture, it started gaining mass at roughly similar temperature as the C_2F (i.e., 520 °C in **Fig. 11B**), reaching a maximum mass of 113wt%. Then as the temperature rose, it experienced two different mass losses at 675

and 760 °C which can be attributed to the C_2F and the free CaO of the C_2F/CaO composite following behaving as expected if by themselves.

Rather than carbonating, coking via the Boudouard reaction $\left(2CO_{(g)} \leftrightharpoons C_{(s)} + CO_{2(g)}\right)$ can be ruled out as an explanation for the mass increase in **Fig. 11A.** The Boudouard reaction has equilibrium constant $\left(\frac{P_{CO_2}}{P_{CO}{}^2}\right)$ [20]. At the inlet condition with $\frac{P_{CO_2}}{P_{CO}{}^2}$ of ~11 bar^{-1}, it is already higher than the equilibrium constant of the Boudouard reaction at 650 °C, i.e., ~3 bar^{-1} [20]. This means that the inlet concentration has already beyond equilibrium. Moreover, CO and CO_2 formation during purging in **Fig. 9A** suggested that the C_2F is reduced and carbonated rather than coking.

Alternatively, C_2F alone is able to carbonate via

$$Ca_2Fe_2O_{5(s)} + 2CO_{2(g)} \leftrightharpoons 2CaCO_{3(s)} + Fe_2O_{3(s)} \qquad \textbf{(R-9)},$$

but at a much lower temperature range than CaO alone, i.e., the equilibrium P_{CO_2} of **R-9** is ~1 bar at 650 – 700 °C [25,34] as shown in **Fig. S13**. However, at these lower temperatures, the carbonation kinetics are very slow. The very small mass gain (0.3wt%) during temperature-programmed carbonation under CO_2 for the as-prepared C_2F in **Fig. S7** was likely from impurity CaO rather than the C_2F. As-prepared C_2F started losing mass at similar temperature when the limestone should be calcined, i.e., > 800 °C.

Given that neither carbonation (**R-9**) nor reduction of the C_2F (**R-5**) should occur directly for the given P_{CO}/P_{CO_2} of the hypothetical BFG, this suggests that instead of following **R-5** and then **R-1** in consecutive steps during reductive-carbonation in the fluidised bed (**Fig. 9A**), CO combustion by C_2F at temperatures which allow a carbonate product proceeds directly via e.g., **R-7**. Alternatively, considering CO_2 is in the feed, reduction to higher oxidation states of

iron is also possible. i.e., linear combinations of **R-5**, **R-1**, and metallic Fe oxidation to higher oxidation states (e.g., Fe_xO, Fe_3O_4), i.e.,

$$Ca_2Fe_2O_{5(s)} + \left(3 - \frac{2}{x}\right)CO_{(g)} + \left(\frac{2}{x} - 1\right)CO_{2(g)} \rightleftharpoons \frac{2}{x}Fe_xO_{(s)} + 2CaCO_{3(s)} \quad \textbf{(R-10)}$$

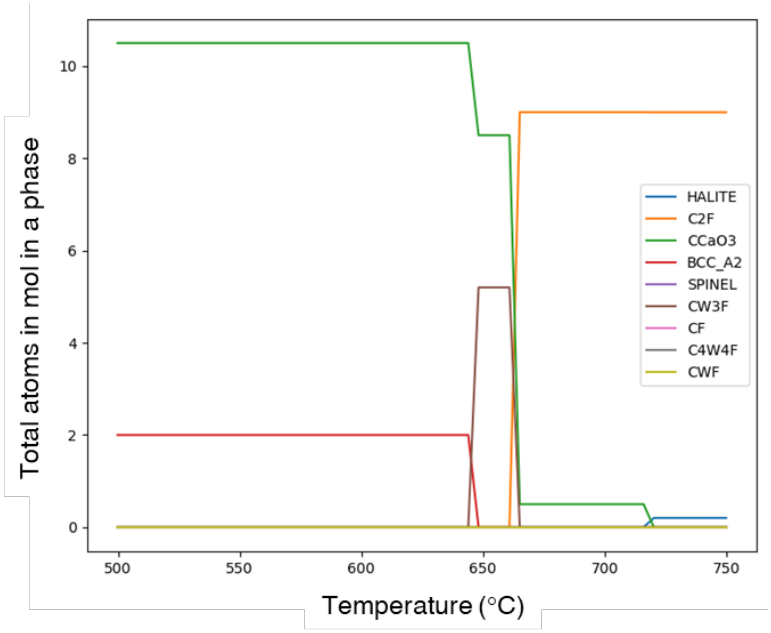
$$Ca_2Fe_2O_{5(s)} + \frac{1}{3}CO_{(g)} + \frac{5}{3}CO_{2(g)} \rightleftharpoons \frac{2}{3}Fe_3O_{4(s)} + 2CaCO_{3(s)} \quad \textbf{(R-11)}.$$

For a partially reduced sample containing Fe, CaO and C_2F, mass transfer limitations could give local conditions in which the P_{CO}/P_{CO_2} is sufficient to allow reduction to proceed via **R-5**, e.g., slow mass transfer of CO and fast carbonation at the surface. However, this cannot explain how the reaction starts. Thus it is likely, that when carbonation is possible reactions **R-7**, **R-10**, or **R-11** take place, allowing reduction at much lower P_{CO}/P_{CO_2} than if **R-5** was followed.

Further evidence for the importance of the carbonation and reduction being coupled is shown in **Fig. S14**. Here the sample is first held under conditions which would reduce any free iron oxide phases, before starting the experiment. As the temperature is reduced, the reduction and carbonation of the C_2F occur simultaneously and are not influenced by the reduction of any impurity phases that might be present.

Fig. 12 shows the phases that should form if the sample reaches equilibrium at each temperature in the experiment shown in **Fig. 11**. At low temperatures, thermodynamics should drive the sample to carbonate and reduce to metallic Fe + $CaCO_3$. In the actual experiment, kinetics prevents this until around 505 °C when the sample begins to carbonate. As seen in **Fig. 12**, there is a narrow window in which it is possible to form calcium ferrites with a lower oxidation state than C_2F. On further heating, the carbonate is decomposed as C_2F forms at 650 – 660 °C in the experiment in **Fig 11A** and **Fig. S11**, vs the thermodynamic prediction of around 665 °C. The calculation in **Fig. 12** included a small amount of excess calcium, and its

539 decomposition to CaO can be seen occurring, as expected, around 720 °C, much higher than if
540 the calcium can form C_2F.



541

542 **Figure 12** TGA experiments of $P_{CO}/P_{CO_2} = 1.3$ and $P_{CO_2} = 0.056$ atm (computed using
543 MTDATA [33], SUB-SGTE database for CO_2 and $CaCO_3$ and HTOX for all other species
544 with Fe:Ca of 2:2.1).

545 Experiments in **Fig. 11** were repeated for different P_{CO}/P_{CO_2} i.e., 0.95 and 0.03 and their
546 expected phases changes throughout the temperature ramp are shown in Supplementary
547 Information **(S9)**. **Fig. S16** shows that at $P_{CO}/P_{CO_2} = 0.95$, when it initially begins to carbonate
548 at 500 °C, the system is driven towards an equilibrium of Fe and $CaCO_3$, and as the temperature
549 rises, this changes to favouring the formation of Fe_xO (i.e., a halite phase + $CaCO_3$). As the
550 temperature increases, there is a window where more complicated ferrites can form, before
551 decomposition to C_2F would result in mass loss (experimentally observed at 670 °C in **Fig. S15**
552 vs 675 °C expected from thermodynamics in **Fig. S16**).

553 The lowest $P_{CO}/P_{CO_2} = 0.03$ follows a similar pattern with the exception that at
554 temperatures where mass gain occurs, magnetite + $CaCO_3$ should form (see **Figs. S17** and **S18**).

There is general agreement between when the mass loss occurs and the thermodynamic prediction for when C_2F forms. The thermal lag effect on decomposition temperatures for C_2F (**Figs. 11A, S15A, S17A**) is less prominent compared to CaO (**Fig. 11C**), considering only small ΔT between exothermic reactions **R-7/R-10/R-11** and their reversed reactions. On the other hand, for CaO, there is at least a ΔT of 200 °C between carbonation and calcination temperatures (see **Figs. 11C** and **S12**), which allows sufficient time for heat to dissipate. The total C_2F conversion for experiments in **Fig. 11A**, **S15A**, and **S17A** were ~27%, 18%, and 25% for the predicted phases of Fe + $CaCO_3$, Fe_xO + $CaCO_3$, and Fe_3O_4 + $CaCO_3$, respectively.

When Fe_xO forms instead of metallic iron, it would add extra endothermicity to the carbonator, given that

$$2Fe_{(s)} + \frac{2}{x}CO_{2(g)} \rightleftharpoons \frac{2}{x}Fe_xO_{(s)} + \frac{2}{x}CO_{(g)} \qquad \textbf{(R-12)}.$$

is endothermic (ΔH of ~35 kJ/mol-C_2F [33,34,56]). Therefore, when C_2F reacts via **R-10** instead of **R-7**, forming Fe_xO+$CaCO_3$, extra endothermicity in the carbonator would result in a greater amount of heat being chemically transferred to the calciner.

Carbonation driving reduction of C_2F was also observed in the fluidised bed results in **Fig. 9A**. If **R-7** can proceed directly as suggested from **Fig. S19** i.e., the phases at equilibrium should be Fe+$CaCO_3$ at given hypothetical BFG composition and at 650 °C, the reduction is no longer limited by the equilibrium P_{CO}/P_{CO_2} for **R-5**. Instead the limiting equilibrium constant is now $k_{p_{\mathbf{R-7}}} = \frac{[P_{CO_2}]}{[P_{CO}]^3}$, which is equal to 174 bar^{-2} (calculated using Barin data book [34] at 630 °C); 215 bar^{-2} at 650 °C (estimated using MTDATA, HTOX and SUB-SGTE [33]). The inlet condition with $\frac{[P_{CO_2}]}{[P_{CO}]^3}$ of 87 bar^{-2} would theoretically allow the **R-7** to proceed. **Fig. 9A(i)** shows that when CO conversion at its highest (t = ~2 min), $\frac{[P_{CO_2}]}{[P_{CO}]^3}$ is 227 which indicates

576 that equilibrium is approached for **R-7**. **Fig. S19** shows that under these conditions only Fe and
577 $CaCO_3$ would be expected, with higher temperatures needed to form other ferrites.

578 Excess CaO from C_2F/CaO composite pulled the equilibrium even further, allowing more
579 CO combustion to occur during the reductive-carbonation step as shown in **Fig. 9B(i)**. The
580 ratio P_{CO}/P_{CO_2} during the reductive-carbonation step in **Fig. 9B(i)** was ~3 for t < 5 min,
581 indicating reduction of C_2F to Fe and CaO was controlling the process (**R-5**). Following this,
582 the P_{CO}/P_{CO_2} dropped to 1.5, suggesting the formation of other phases. At t > 20 min, the
583 system had returned to the inlet P_{CO}/P_{CO_2} of 1.3. This indicates that when excess CaO is
584 available to capture CO_2, the reaction might follow **R-1** and **R-5** where C_2F is reduced forming
585 metallic Fe + CaO. However, when the rate of carbonation of the free CaO falls as it begin to
586 run out, the C_2F is then reduced to Fe + $CaCO_3$ via **R-7**.

587 Excess CaO in the C_2F/CaO can improve the overall carbon removal (see **Fig. 10**) as well
588 as total CO converted. According to the measured oxygen transfer, C_2F conversion only
589 reached 9% during reductive-carbonation step in the fluidised bed in **Fig. 9**, whilst C_2F/CaO
590 and C_2F+limestone conversions were 32% and 8% in respect to total C_2F amount in the sample,
591 respectively (average for 3 cycles). In spite of relatively higher carbonation of the
592 C_2F+limestone (0.09 g-CO_2/g-material) compared to C_2F (0.04 g-CO_2/g-material), the
593 C_2F+limestone had much less reduction compared to the C_2F/CaO composite and had similar
594 C_2F conversion with C_2F alone.

595 It appears that the close proximity between the available CaO and the C_2F better assists
596 the enhanced combustion reaction. Excess CaO has the effect of lowering the bulk CO_2
597 concentration, and if carbonation is fast enough, might also give a higher local P_{CO}/P_{CO_2} ratio
598 at the particle surface if there is any mass transfer limitation. The effect of the excess CaO is
599 therefore a physical effect of the lowering of the CO_2 partial pressure, that subsequently

600 changes driving force for reduction of the C_2F. This is consistent with the fact that the excess
601 CaO within the composite (when carbonated) behaves similar to limestone, with similar
602 decomposition temperatures as shown in **Fig. 4** and **11**. Therefore, the benefit of lowering the
603 decarbonation temperature by utilising the mixed phase C_2F is diminished, though, being
604 endothermic when reduced in CO, C_2F reduction in the carbonator would still benefit the
605 overall system.

606

607 **6. Conclusion**

608 In this work, $Ca_2Fe_2O_5$ (C_2F) demonstrates promising performance when removing CO
609 and CO_2 from a BFG via integrated Ca-looping and chemical looping combustion (CaL-CLC).
610 The low P_{O_2} property of the metal oxide favours endothermic reaction in combusting CO/H_2,
611 allowing combustible gases in the BFG to be utilised. The heat is stored as a chemical reaction
612 to be released during the regeneration step in the calciner.

613 When C_2F reacts with CO at high temperature (e.g., 900 °C), it follows $Ca_2Fe_2O_{5(s)} +$
614 $3CO_{(g)} \leftrightharpoons 2CaO_{(s)} + 2Fe_{(s)} + 3CO_{2(g)}$ whose P_{CO}/P_{CO_2} is ~3. Therefore, the C_2F would not
615 combust CO from the BFG with P_{CO}/P_{CO_2} of ~1. However, at temperature at which CaO could
616 carbonate, instead of following sequential reaction of (i) C_2F reduction to CaO+Fe and (ii) CaO
617 carbonation to $CaCO_3$, the C_2F follows a direct reductive-carbonation mechanism route of, e.g.,

$$Ca_2Fe_2O_{5(s)} + 3CO_{(g)} \leftrightharpoons 2CaCO_{3(s)} + 2Fe_{(s)} + CO_{2(g)}$$

$$Ca_2Fe_2O_{5(s)} + (3 - 2/x)CO_{(g)} + (2/x - 1)CO_{2(g)} \rightleftharpoons 2/x\, Fe_xO_{(s)} + 2CaCO_{3(s)}$$

$$Ca_2Fe_2O_{5(s)} + 1/3\, CO_{(g)} + 5/3\, CO_{2(g)} \rightleftharpoons 2/3\, Fe_3O_{4(s)} + 2CaCO_{3(s)}.$$

618 The formation of phases at equilibrium are controlled by temperature, P_{O_2} (P_{CO}/P_{CO_2}),
619 and P_{CO_2}. The direct reductive-carbonation pathway allows the C_2F to simultaneously combust

620 CO and capture CO_2 from the hypothetical BFG in the fluidised bed. Here, adding extra CaO
621 to C_2F as a composite (C_2F/CaO) or separate particle (C_2F+limestone) were compared with the
622 C_2F alone. The composite had better oxygen transfer and CO_2 capture compared to the C_2F and
623 C_2F+limestone.

624 Incorporation of reduced-carbonated C_2F drives the decomposition of $CaCO_3$, allowing it
625 to decompose at much lower temperature than the CaO alone. In general, the decomposition
626 temperature of the reduced-carbonated C_2F at various P_{CO}/P_{CO_2} agrees with thermodynamics
627 prediction from MTDATA.

628

629 **CRediT authorship contribution statement**

630 **M.S. Sukma:** Conceptualisation, data curation, formal analysis, investigation, writing –
631 original, methodology, validation. **Y. Zheng:** Conceptualisation, writing – review and editing.
632 **S.A. Scott:** Funding acquisition, conceptualisation, supervision, validation, writing – review
633 and editing, project administration, methodology, validation.

634 **Associated Content**

635 **Data**

636 All data for this work is provided within the paper, the associated supporting information,
637 and on the repository https://www.repository.cam.ac.uk/.

638 **Author Information**

639 **Author**

640 **Made Santihayu Sukma** – Energy Laboratory, Department of Engineering, University of
641 Cambridge, Trumpington Street, Cambridge, CB2 1PZ, United Kingdom. Tel.:
642 +447472349105. Email: mss82@cam.ac.uk.

Corresponding Author

Stuart Ashley Scott – Energy Laboratory, ISO-45, Department of Engineering, University of Cambridge, Trumpington Street, Cambridge, CB2 1PZ, United Kingdom. Tel.: +441223332645. Email: sas37@cam.ac.uk.

Author

Yaoyao Zheng – Energy Laboratory, Department of Engineering, University of Cambridge, Trumpington Street, Cambridge, CB2 1PZ, United Kingdom. | Faculty of Engineering, University of Nottingham, Triump Road, Nottingham, NG8 1BB, United Kingdom

Declaration of competing interest

The authors declare no competing financial interest.

Acknowledgement

M.S. Sukma is very grateful to the Indonesian Endowment Fund for Education (LPDP) Scholarship and Government of Indonesia for the financial support given during her PhD study. The authors acknowledge the EPRSC project (BREINSTORM - EP/S030387/1) for providing funding and support to this study. We would like to thank Mr Harry Druiff for the help with XRD tests.

References

[1] K. He, L. Wang, A review of energy use and energy-efficient technologies for the iron and steel industry, Renew. Sustain. Energy Rev. 70 (2017) 1022–1039. https://doi.org/10.1016/j.rser.2016.12.007.

[2] N. Margolis, L. Sousa, Energy and environmental profile of the U.S. iron and steel industry, Proc. ACEEE Summer Study Energy Effic. Ind. (1997) 103–113.

[3] Environmental Protection Agency, Available and Emerging Technologies for Reducing Greenhouse Gas Emissions From the Iron and Steel Industry, (2012) 78. https://doi.org/10.1016/0026-0495(93)90015-G.

[4] International Energy Agency, Iron and Steel Technology Roadmap, Iron Steel Technol. Roadmap. (2020). https://doi.org/10.1787/3dcc2a1b-en.

[5] A. Carpenter, CO_2 abatement in the iron and steel industry, London, UK, 2012. www.elsevier.com/locate/enconman.

[6] S. Caillat, Burners in the steel industry: Utilization of by-product combustion gases in reheating furnaces and annealing lines, Energy Procedia. 120 (2017) 20–27. https://doi.org/10.1016/j.egypro.2017.07.152.

[7] M. Erans, V. Manovic, E.J. Anthony, Calcium looping sorbents for CO2 capture, Appl. Energy. 180 (2016) 722–742. https://doi.org/10.1016/j.apenergy.2016.07.074.

[8] T. Shimizu, T. Hirama, H. Hosoda, K. Kitano, M. Inagaki, K. Tejima, A twin fluid-bed reactor for removal of CO2 from combustion processes, Chem. Eng. Res. Des. 77 (1999) 62–68. https://doi.org/10.1205/026387699525882.

[9] M. Ishida, D. Zheng, T. Akehata, Evaluation of a chemical-looping-combustion power-generation system by graphic exergy analysis, Energy. 12 (1987) 147–154. https://doi.org/10.1016/0360-5442(87)90119-8.

[10] M. Ishida, H. Jin, T. Okamoto, A fundamental study of a new kind of medium material for chemical-looping combustion, Energy and Fuels. 10 (1996) 958–963. https://doi.org/10.1021/ef950173n.

688 [11] M. Ishida, H. Jin, A novel chemical-looping combustor without NOx formation, Ind.
689 Eng. Chem. Res. 35 (1996) 2469–2472. https://doi.org/10.1021/ie950680s.

690 [12] H. Gu, G. Song, M. Niu, S. Zhao, Y. Gao, F. Li, Sr2CeO4 as a robust high temperature
691 sorbent for CO2 capture with near 100% sorbent conversion efficiency, Chem. Eng. J.
692 441 (2022) 135942. https://doi.org/10.1016/j.cej.2022.135942.

693 [13] P.S. Fennell, R. Pacciani, J.S. Dennis, J.F. Davidson, A.N. Hayhurst, The effects of
694 repeated cycles of calcination and carbonation on a variety of different limestones, as
695 measured in a hot fluidized bed of sand, Energy and Fuels. 21 (2007) 2072–2081.
696 https://doi.org/10.1021/ef060506o.

697 [14] W. Liu, J.S. Dennis, D.S. Sultan, S.A.T. Redfern, S.A. Scott, An investigation of the
698 kinetics of CO 2 uptake by a synthetic calcium based sorbent, Chem. Eng. Sci. 69 (2012)
699 644–658. https://doi.org/10.1016/j.ces.2011.11.036.

700 [15] J.C. Abanades, D. Alvarez, Conversion limits in the reaction of CO2 with lime, Energy
701 and Fuels. 17 (2003) 308–315. https://doi.org/10.1021/ef020152a.

702 [16] S. Tian, J. Jiang, F. Yan, K. Li, X. Chen, Synthesis of Highly Efficient CaO-Based, Self-
703 Stabilizing CO2 Sorbents via Structure-Reforming of Steel Slag, Environ. Sci. Technol.
704 49 (2015) 7464–7472. https://doi.org/10.1021/acs.est.5b00244.

705 [17] J. Ma, D. Mei, W. Peng, X. Tian, D. Ren, H. Zhao, On the high performance of a core-
706 shell structured CaO-CuO/MgO@Al2O3 material in calcium looping integrated with
707 chemical looping combustion (CaL-CLC), Chem. Eng. J. 368 (2019) 504–512.
708 https://doi.org/10.1016/j.cej.2019.02.188.

709 [18] A. Perejón, L.M. Romeo, Y. Lara, P. Lisbona, A. Martínez, J.M. Valverde, The
710 Calcium-Looping technology for CO2 capture: On the important roles of energy

711 integration and sorbent behavior, Appl. Energy. 162 (2016) 787–807.
712 https://doi.org/10.1016/j.apenergy.2015.10.121.

713 [19] S. Tian, K. Li, J. Jiang, X. Chen, F. Yan, CO2 abatement from the iron and steel industry
714 using a combined Ca-Fe chemical loop, Appl. Energy. 170 (2016) 345–352.
715 https://doi.org/10.1016/j.apenergy.2016.02.120.

716 [20] S. McBride, B., Zehe, M., Gordon, NASA Glenn Coefficients for Calculating
717 Thermodynamic Properties of Individual Species, 2002. https://doi.org/NASA Report:
718 TP-2002-211556.

719 [21] M. Bui, C.S. Adjiman, A. Bardow, E.J. Anthony, A. Boston, S. Brown, P.S. Fennell, S.
720 Fuss, A. Galindo, L.A. Hackett, J.P. Hallett, H.J. Herzog, G. Jackson, J. Kemper, S.
721 Krevor, G.C. Maitland, M. Matuszewski, I.S. Metcalfe, C. Petit, G. Puxty, J. Reimer,
722 D.M. Reiner, E.S. Rubin, S.A. Scott, N. Shah, B. Smit, J.P.M. Trusler, P. Webley, J.
723 Wilcox, N. Mac Dowell, Carbon capture and storage (CCS): The way forward, Energy
724 Environ. Sci. 11 (2018) 1062–1176. https://doi.org/10.1039/c7ee02342a.

725 [22] J.C. Abanades, R. Murillo, J.R. Fernandez, G. Grasa, I. Martínez, New CO2 capture
726 process for hydrogen production combining Ca and Cu chemical loops, Environ. Sci.
727 Technol. 44 (2010) 6901–6904. https://doi.org/10.1021/es101707t.

728 [23] N. MacDowell, N. Florin, A. Buchard, J. Hallett, A. Galindo, G. Jackson, C.S. Adjiman,
729 C.K. Williams, N. Shah, P. Fennell, An overview of CO2 capture technologies, Energy
730 Environ. Sci. 3 (2010) 1645–1669. https://doi.org/10.1039/c004106h.

731 [24] M. Ismail, W. Liu, M.T. Dunstan, S.A. Scott, Development and performance of iron
732 based oxygen carriers containing calcium ferrites for chemical looping combustion and
733 production of hydrogen, Int. J. Hydrogen Energy. 41 (2016) 4073–4084.
734 https://doi.org/10.1016/j.ijhydene.2015.11.066.

735 [25] M. Ismail, W. Liu, M.S.C. Chan, M.T. Dunstan, S.A. Scott, Synthesis, Application, and
736 Carbonation Behavior of Ca2Fe2O5 for Chemical Looping H2 Production, Energy and
737 Fuels. 30 (2016) 6220–6232. https://doi.org/10.1021/acs.energyfuels.6b00631.

738 [26] N.L. Galinsky, A. Shafiefarhood, Y. Chen, L. Neal, F. Li, Effect of support on redox
739 stability of iron oxide for chemical looping conversion of methane, Appl. Catal. B
740 Environ. 164 (2015) 371–379. https://doi.org/10.1016/j.apcatb.2014.09.023.

741 [27] T. Mattisson, A. Lyngfelt, P. Cho, The use of iron oxide as an oxygen carrier in
742 chemical-looping combustion of methane with inherent separation of CO2, Fuel. 80
743 (2001) 1953–1962. https://doi.org/10.1016/S0016-2361(01)00051-5.

744 [28] Z. Cheng, L. Qin, J.A. Fan, L.S. Fan, New Insight into the Development of Oxygen
745 Carrier Materials for Chemical Looping Systems, Engineering. 4 (2018) 343–351.
746 https://doi.org/10.1016/j.eng.2018.05.002.

747 [29] V. Manovic, Y. Wu, I. He, E.J. Anthony, Core-in-shell CaO/CuO-based composite for
748 CO2 capture, Ind. Eng. Chem. Res. 50 (2011) 12384–12391.
749 https://doi.org/10.1021/ie201427g.

750 [30] A.M. Kierzkowska, C.R. Müller, Development of calcium-based, copper-functionalised
751 CO 2 sorbents to integrate chemical looping combustion into calcium looping, Energy
752 Environ. Sci. 5 (2012) 6061–6065. https://doi.org/10.1039/c2ee03079a.

753 [31] J.R. Fernández, V. Spallina, J.C. Abanades, Advanced Packed-Bed Ca-Cu Looping
754 Process for the CO2 Capture From Steel Mill Off-Gases, Front. Energy Res. 8 (2020)
755 1–13. https://doi.org/10.3389/fenrg.2020.00146.

756 [32] V. Manovic, E.J. Anthony, Integration of calcium and chemical looping combustion
757 using composite CaO/CuO-based materials, Environ. Sci. Technol. 45 (2011) 10750–

758 10756. https://doi.org/10.1021/es202292c.

759 [33] R.H. Davies, A.T. Dinsdale, J.A. Gisby, J.A.J. Robinson, S.M. Martin, MTDATA -
760 Thermodynamic and phase equilibrium software from the national physical laboratory,
761 Calphad Comput. Coupling Phase Diagrams Thermochem. 26 (2002) 229–271.
762 https://doi.org/10.1016/S0364-5916(02)00036-6.

763 [34] I. Barin, Thermochemical Data of Pure Substances (3rd Ed.), VCH Verlagsgesellschaft,
764 Weinheim, Germany, 1995.

765 [35] M. Ismail, W. Liu, M.T. Dunstan, S.A. Scott, Development and performance of iron
766 based oxygen carriers containing calcium ferrites for chemical looping combustion and
767 production of hydrogen, Int. J. Hydrogen Energy. 41 (2016) 4073–4084.
768 https://doi.org/10.1016/j.ijhydene.2015.11.066.

769 [36] M.S.C. Chan, W. Liu, M. Ismail, Y. Yang, S.A. Scott, J.S. Dennis, Improving hydrogen
770 yields, and hydrogen: Steam ratio in the chemical looping production of hydrogen using
771 Ca2Fe2O5, Chem. Eng. J. 296 (2016) 406–411.
772 https://doi.org/10.1016/j.cej.2016.03.132.

773 [37] D. Hosseini, F. Donat, P.M. Abdala, S.M. Kim, A.M. Kierzkowska, C.R. Müller,
774 Reversible Exsolution of Dopant Improves the Performance of Ca2Fe2O5 for Chemical
775 Looping Hydrogen Production, ACS Appl. Mater. Interfaces. 11 (2019) 18276–18284.
776 https://doi.org/10.1021/acsami.8b16732.

777 [38] C.D. Bohn, C.R. Müller, J.P. Cleeton, A.N. Hayhurst, J.F. Davidson, S.A. Scott, J.S.
778 Dennis, Production of very pure hydrogen with simultaneous capture of carbon dioxide
779 using the redox reactions of iron oxides in packed beds, Ind. Eng. Chem. Res. 47 (2008)
780 7623–7630. https://doi.org/10.1021/ie800335j.

781 [39] C.D. Bohn, J.P. Cleeton, C.R. Müller, S.Y. Chuang, S.A. Scott, J.S. Dennis, Stabilizing
782 iron oxide used in cycles of reduction and oxidation for hydrogen production, Energy
783 and Fuels. 24 (2010) 4025–4033. https://doi.org/10.1021/ef100199f.

784 [40] W. Liu, J.S. Dennis, S.A. Scott, The effect of addition of ZrO2 to Fe2O3 for hydrogen
785 production by chemical looping, Ind. Eng. Chem. Res. 51 (2012) 16597–16609.
786 https://doi.org/10.1021/ie302626x.

787 [41] Q. Imtiaz, N.S. Yüzbasi, P.M. Abdala, A.M. Kierzkowska, W. Van Beek, M. Broda,
788 C.R. Müller, Development of MgAl2O4-stabilized, Cu-doped, Fe2O3-based oxygen
789 carriers for thermochemical water-splitting, J. Mater. Chem. A. 4 (2015) 113–123.
790 https://doi.org/10.1039/c5ta06753g.

791 [42] H.C. Wu, Y. Ku, Enhanced performance of chemical looping combustion of methane
792 with Fe2O3/Al2O3/TiO2 oxygen carrier, RSC Adv. 8 (2018) 39902–39912.
793 https://doi.org/10.1039/c8ra07863g.

794 [43] Z. Zhou, G. Deng, L. Li, X. Liu, Z. Sun, L. Duan, Chemical looping co-conversion of
795 CH4 and CO2 using Fe2O3/Al2O3 pellets as both oxygen carrier and catalyst in a
796 fluidized bed reactor, Chem. Eng. J. 428 (2021) 132133.
797 https://doi.org/10.1016/j.cej.2021.132133.

798 [44] J. Huang, Y. Fu, S. Li, W. Kong, J. Zhang, Y. Sun, Enhanced activity of Mg-Fe-O
799 ferrites for two-step thermochemical CO 2 splitting, J. CO2 Util. 27 (2018) 450–458.
800 https://doi.org/10.1016/j.jcou.2018.08.007.

801 [45] Q. Fan, C. Huang, S. Xi, Y. Yan, J. Huang, S. Saqline, L. Tao, Y. Dai, A. Borgna, X.
802 Wang, W. Liu, Breaking the Stoichiometric Limit in Oxygen-Carrying Capacity of Fe-
803 Based Oxygen Carriers for Chemical Looping Combustion using the Mg-Fe - O Solid
804 Solution System, (2022). https://doi.org/10.1021/acssuschemeng.2c00271.

[46] Z. Sun, S. Chen, J. Hu, A. Chen, A.H. Rony, C.K. Russell, W. Xiang, M. Fan, M. Darby Dyar, E.C. Dklute, Ca2Fe2O5: A promising oxygen carrier for CO/CH4 conversion and almost-pure H2 production with inherent CO2 capture over a two-step chemical looping hydrogen generation process, Appl. Energy. 211 (2018) 431–442. https://doi.org/10.1016/j.apenergy.2017.11.005.

[47] M.S. Sukma, Y. Zheng, P. Hodgson, S.A. Scott, Understanding the Behavior of Dicalcium Ferrite (Ca 2 Fe 2 O 5) in Chemical Looping Syngas Production from CH 4, Energy & Fuels. 36 (2022) 9410–9422. https://doi.org/10.1021/acs.energyfuels.2c01065.

[48] D.D. Miller, J. Riley, R. Siriwardane, Interaction of Methane with Calcium Ferrite in the Chemical Looping Partial Oxidation Application: Experimental and DFT Study, Energy and Fuels. 34 (2020) 2193–2204. https://doi.org/10.1021/acs.energyfuels.9b03623.

[49] S.M. Kim, A. Armutlulu, A.M. Kierzkowska, D. Hosseini, F. Donat, C. Müller, Development of an effective bi-functional Ni-CaO catalyst-sorbent for the sorption-enhanced water gas shift reaction through structural optimization and the controlled deposition of a stabilizer by atomic layer deposition, Sustain. Energy Fuels. 4 (2020) 713–729. https://doi.org/10.1039/c9se00619b.

[50] Y. Zheng, M.S. Sukma, S.A. Scott, The exploration of NiO/Ca2Fe2O5/CaO in chemical looping methane conversion for syngas and H2 production, Chem. Eng. J. 465 (2023) 142779. https://doi.org/10.1016/j.cej.2023.142779.

[51] H. Gu, G. Song, M. Niu, S. Zhao, Y. Gao, F. Li, Sr2CeO4 as a robust high temperature sorbent for CO2 capture with near 100% sorbent conversion efficiency, Chem. Eng. J. 441 (2022) 135942. https://doi.org/10.1016/j.cej.2022.135942.

[52] S.M. Kim, A. Armutlulu, A.M. Kierzkowska, C.R. Müller, Inverse Opal-Like, Ca3Al2O6-Stabilized, CaO-Based CO2 Sorbent: Stabilization of a Highly Porous Structure to Improve Its Cyclic CO2 Uptake, ACS Appl. Energy Mater. 2 (2019) 6461–6471. https://doi.org/10.1021/acsaem.9b01058.

[53] L. Li, D.L. King, Z. Nie, C. Howard, Magnesia-stabilized calcium oxide absorbents with improved durability for high temperature CO2 capture, Ind. Eng. Chem. Res. 48 (2009) 10604–10613. https://doi.org/10.1021/ie901166b.

[54] H. Sun, C. Wu, B. Shen, X. Zhang, Y. Zhang, J. Huang, Progress in the development and application of CaO-based adsorbents for CO2 capture—a review, Mater. Today Sustain. 1–2 (2018) 1–27. https://doi.org/10.1016/j.mtsust.2018.08.001.

[55] E.H. Baker, The Calcium Oxide-Carbon Dioxide System in the Pressure Range 1−300 atm, J. Chem. Soc. (1962) 464−470.

[56] R.L. Wagman, D.D., Evans, W.H., Parker, V.B., Schumm, R.H., Halow, I., Bailey, S.M., Churney, K.L., and Nuttall, The NBS Tables of Chemical Thermodynamic properties: Selected values for inorganic and C1 and C2 organic substances in SI units, J. Phys. Chem. Ref. Data. 11 (1982).